



HAL
open science

Fractional-Order Integral Terminal Sliding-Mode Control for Perturbed Nonlinear Systems With Application to Quadrotors

Moussa Labbadi, Michael Defoort, Gian Paolo Incremona, Mohamed Djemai

► **To cite this version:**

Moussa Labbadi, Michael Defoort, Gian Paolo Incremona, Mohamed Djemai. Fractional-Order Integral Terminal Sliding-Mode Control for Perturbed Nonlinear Systems With Application to Quadrotors. *International Journal of Robust and Nonlinear Control*, 2023, Special Issue: Advanced Control and Estimation applied to Aerial Robotic Vehicles, 33 (17), pp.10278-10303. 10.1002/rnc.6608 . hal-04068247

HAL Id: hal-04068247

<https://hal.univ-grenoble-alpes.fr/hal-04068247v1>

Submitted on 13 Apr 2023

HAL is a multi-disciplinary open access archive for the deposit and dissemination of scientific research documents, whether they are published or not. The documents may come from teaching and research institutions in France or abroad, or from public or private research centers.

L'archive ouverte pluridisciplinaire **HAL**, est destinée au dépôt et à la diffusion de documents scientifiques de niveau recherche, publiés ou non, émanant des établissements d'enseignement et de recherche français ou étrangers, des laboratoires publics ou privés.

ARTICLE TYPE

Fractional-Order Integral Terminal Sliding-Mode Control for Perturbed Nonlinear Systems With Application to Quadrotors

M. Labbadi*¹ | M. Defoort² | G. P. Incremona³ | M. Djemai^{2,4}

¹ Univ. Grenoble Alpes, CNRS, Grenoble INP, GIPSA-lab, 38000 Grenoble, France, France

² Univ. Polytechnique Hauts-de-France, INSA Hauts-de-France, LAMIH, CNRS, UMR 8201, F-59313 Valenciennes, France

³ Dipartimento di Elettronica, Informazione e Bioingegneria, Politecnico di Milano, Piazza Leonardo da Vinci 32, 20133, Milano, Italy

⁴ QUARTZ Laboratory EA 7393. ENSEA Cergy 6 Avenue du Ponceau, 95000 Cergy, France

Correspondence

*Corresponding author Moussa Labbadi, Corresponding address. Email: moussa.labbadi@gipsa-lab.grenoble-inp.fr

Present Address

Univ. Grenoble Alpes, CNRS, Grenoble INP, GIPSA-lab, 38000 Grenoble, France

Abstract

In this paper, a novel fractional-order recursive integral terminal sliding mode (FORITSM) control is proposed for nonlinear systems in the presence of external disturbances with unknown bounds. The proposed control approach provides an easy-to-implement solution capable of zeroing the sliding variable in a finite-time (FnT) by adding a fractional-order command filter. Moreover, the reaching phase is eliminated, and FnT convergence of the system states is proved. The proposed technique has also a chattering alleviation property, which is beneficial for practical cases, as the control of quadrotor UAVs presented in the paper. Finally, a simulation case study on a quadrotor system is illustrated to show the effectiveness of the proposed FORITSM control, also with respect to classical methods.

KEYWORDS:

Chattering alleviation, FnT, fractional-order recursive integral terminal sliding mode, full-order sliding mode, reaching phase, uncertain systems.

1 | INTRODUCTION

Sliding mode control (SMC) is a powerful easy-to-implement control technique with remarkable robustness properties in case of systems affected by disturbances and unavoidable modelling uncertainties^{1,2,4}. The goal of SMC in its classical version is to compel the behavior of a dynamical system according to a manifold, i.e., the so-called “sliding surface”, specified by a function known as “sliding variable”, via a discontinuous controller depending on the sliding variable itself.

Once the sliding variable is zeroed, that is a “sliding mode” is enabled, it can be proved that the controlled system is insensitive to the uncertainty terms fulfilling a matched condition. Moreover, the key feature of the SMC method is the capability to enable a finite-time convergence of the sliding variable towards the sliding surface, thus implying an equivalent reduced order dynamics, for which asymptotic stability of the system trajectories is guaranteed. However, more recently, advanced techniques extended the original SMC concept by enhancing the robustness properties of the controlled system through the introduction of integral methods³, or by introducing state constraints⁵, or enabling also a FnT convergence of the system trajectories by using terminal sliding modes⁷.

1.1 | Background and motivations

In this paper, we consider the family of the terminal sliding mode (TSM) controllers. As previously mentioned, this type of control law guarantees that, if the sliding mode exists, this allows to regulate the system trajectories in FnT. Nevertheless, the

main drawback of TSM is the occurrence of singularity in the control signal, which could cause system instability⁸. Specifically, in⁸ such technical concerns and future challenges have been discussed in the perspective of a broader scope of technological advances such as cyber-physical systems, artificial intelligence, and network systems, providing a summary of the state of the art in TSM control theory and applications.

To avoid the singularity problem, nonsingular TSM (NTSM) controllers have been developed in recent years, see⁹ or¹¹, where a finite-time stabilizing method based on the SMC strategy was devised to handle this issue. Aside from singularity, TSM and NTSM control approaches suffer the generation of chattering phenomenon due to the discontinuity of the control function, resulting in high-frequency oscillations of the system states, which can damage mechanical components and lead to input saturation when employed in nonlinear systems^{10,12}.

Several methods have been introduced in the literature for reducing chattering, including the boundary layer method¹³, the high-order sliding-mode method^{14,15}, and the disturbance estimation method¹⁶. In the case of boundary layer approach, the saturation function or sigmoid function are adopted. This choice gives rise to a "pseudo-sliding mode", since only a vicinity of the sliding surface is reached, thus possibly causing the loss of robustness of the system in front of disturbances. As for high-order sliding-mode (HOSM) control approaches, they allow to confine the discontinuity to the derivative of the control input while the signal actually fed into the plant is continuous. The disturbance estimation method is instead based on the design of an asymptotic disturbance observer to compensate for the disturbance, thus allowing a smoother control signal¹⁶. Among many other approaches, recently, the combination of internal model principle and adaptive sliding mode control, as proposed in⁶, allows a reduction of the control authority to dominate the uncertainties with a consequent chattering reduction.

Another drawback of the presented SMCs is the length of the reaching phase (RP) and the sensitivity of the controlled system to perturbation during such an interval. Many works have been developed to address these problems, see e.g.,^{18,19,20}. As for integral HOSM controllers, these are instead discussed in²¹ for uncertain nonlinear systems to remove the RP, although the input singularity generated by the sliding function is not studied in depth.

Moreover, to avoid the problem of "complexity explosion", command filtering can be used. For example, in²² a command filtered and adaptive control is proposed, while a command filter-using fractional-order dynamics in the design of sliding mode manifold is presented in^{23,24}. A command filtered based-backstepping technique is suggested in²⁷, and a FnT adaptive control is developed in²⁸. Also command-filter-based adaptive fuzzy FnT control approaches have been proposed as those in^{25,26,28}.

The second part of the paper addresses the tracking control of quadrotors subject to complex disturbances using the proposed command-filter method. Many existing control approaches for the quadrotors system have been proposed in the literature review, for example, in the paper²⁹, an adaptive recursive sliding mode control was designed to achieves a finite time stability with online estimation of the unknown disturbances. The authors of³⁰ proposed a nonlinear implicit PID with feedback gains to reject constant perturbations of unknown magnitude, where the optimal feedback gains are solved by linear matrix inequalities. In³¹, model predictive contouring control was used to obtain optimal quadrotor flight takes. Similarly, the work³² presented a comparative study of nonlinear-model-predictive and differential-flatness-based controllers for quadrotor system. The work developed in³³ proposed a model-free control with time-prescribed convergence taking out uncertainties and disturbances. In³⁴, a robust-integral-signum-error was developed to compensate for the external disturbances. Reference³⁵ combined neural network with backstepping technique for quadrotor landing. In³⁶, a robust control algorithm was designed to address to the autonomous landing problem of quadrotor UAV on mobile platform. Paper³⁷ proposed a recursive SMC based on nonlinear extended state observer (ESO) for the trajectory tracking of 6-DOF hierarchical with external disturbances and uncertainties. In³⁹, a non-singular terminal sliding mode controller was applied to follow desired quadrotor's position. Similarly,³⁸ proposed a finite-time sliding-mode observer to estimate the full state and recognize uniformly Lipschitz disturbances. The authors of⁴⁰ developed a control strategy for autonomous quadrotor vehicle with external disturbances using SMC and backstepping approaches. In⁴¹, an intelligent control strategy based on reinforcement learning was developed for quadrotor vehicle.

1.2 | Contributions

This main contribution of this paper is the design of a novel robust fractional-order FnT control for perturbed nonlinear systems, capable of alleviating chattering phenomena and without singularity. Differently from the existing literature, where a reduction of the reaching phase is adopted^{9,10}, here, making reference to¹², a command-filter based fractional-order (FO) recursive non-singular terminal SMC is presented for the first time, to the best of the authors' knowledge. By employing the fractional-order of the input in the controller, chattering reduction of the input is achieved. In the presence of external perturbations, the presented Lyapunov-based analysis shows that the system trajectories under the proposed control action can converge to the origin in FnT.

Finally, to assess the proposed strategy in a practical example, a quadrotor dynamics is considered and several simulations in different scenarios are provided. Overall, more in detail, the contributions of this paper are summarized as follows:

- (i) To improve the convergence of the standard integer-order FnT command filter and avoid an “explosion of complexity”, a fractional-order finite-time command filter based on recursive nonsingular terminal SMC is introduced for full-order nonlinear system.
- (ii) The fractional-order control input is produced in a nonsingular fractional-order integral form rather than a standard signum function, which is useful for reducing control input chattering. Furthermore, when compared to integral HOSM controllers¹⁷, the FORITSM control only has two layers of sliding manifolds, which makes it easier to build for high-order systems.
- (iii) Based on this fractional-order recursive structure of the control law, the RP is eliminated, thus enhancing the robustness of the controlled system.
- (iv) The proposed control method has been applied for quadrotor dynamics and compared with the work developed in¹².

1.3 | Outline of the paper

The paper is organized as follows. After some preliminaries and the problem statement in Section 2, the main results on the proposed fractional-order finite-time control are given in Section 3. The application to the tracking control problem for a quadrotor dynamics is addressed in Section 4, while simulations are illustrated in Section 5. Finally, some conclusions are gathered in Section 6.

Notation

The main notation and operators used in the paper are hereafter recalled. Let $x \in \mathbb{R}$, then the absolute value of x , denoted by $|x|$, is defined as $|x| = x$ if $x \geq 0$, and $|x| = -x$ if $x < 0$. The function $\text{sign}(x)$ is defined as $\text{sign}(x) = 1$ for $x > 0$, $\text{sign}(x) = -1$ for $x < 0$, and $\text{sign}(x) = 0$ for $x = 0$. For $\gamma \geq 0$, one has that $\text{sig}^\gamma(x) = |x|^\gamma \text{sign}(x)$, so that $\text{sig}^0(x) = \text{sign}(x)$.

2 | PRELIMINARIES AND PROBLEM FORMULATION

In this section, some preliminaries on fractional calculus and Mittag-leffler functions are recalled. Then, the considered control problem is formulated.

2.1 | Preliminaries on fractional calculus

Let us recall some definitions concerning fractional order derivatives. For any real number $\alpha > 0$ (namely, the derivative order), the Riemann-Liouville fractional derivative for a function $\Psi : [a, \infty) \rightarrow \mathbb{R}$ is given by^{42,43}

$${}^RL D_t^\alpha \Psi(t) = \frac{1}{\Gamma(\Upsilon - \alpha)} \frac{d^\Upsilon}{dt^\Upsilon} \int_a^t \frac{\Psi(\tau)}{(t - \tau)^{\alpha - \Upsilon + 1}} d\tau, \quad (1)$$

where $\Upsilon \in \mathbb{N}^*$ is such that $(\Upsilon - 1) < \alpha < \Upsilon$ and $\Gamma(\cdot)$ is the Gamma function expressed as

$$\Gamma(K) = \int_0^\infty e^{-t} t^{K-1} dt. \quad (2)$$

Furthermore, for any real number $\alpha > 0$, the Caputo fractional derivative (CFD) for a function $\Psi : [a, \infty) \rightarrow \mathbb{R}$ is given by^{43,44}

$${}^C D_t^\alpha \Psi(t) = \frac{1}{\Gamma(\alpha - \Upsilon)} \int_a^t \frac{\Psi^{(\Upsilon)}(\tau)}{(t - \tau)^{\alpha - \Upsilon + 1}} d\tau. \quad (3)$$

Some important properties are recalled hereafter.

Property 1. For any real numbers $\alpha \geq \lambda \geq 0$, the CFD for a function $\Psi : [t_0, \infty) \rightarrow \mathbb{R}$ satisfies

$${}^C D_t^\alpha ({}^C D_t^{-\lambda} \Psi(t)) = {}^C D_t^{\alpha-\lambda} \Psi(t). \quad (4)$$

Property 2. Let $0 < \alpha < 1$ and $\Psi : [t_0, \infty) \rightarrow \mathbb{R}$, then the following equality holds:

$${}^C D_t^{1-\alpha} ({}^C D_t^\alpha \Psi(t)) = {}^C D_t^\alpha ({}^C D_t^{1-\alpha} \Psi(t)) = \dot{\Psi}(t). \quad (5)$$

In the following, the operator ${}^C D_t^\alpha$ will be replaced by D^α throughout this paper.

2.2 | Mittag-Leffler type functions

The Mittag-Leffler function^{42,43} can be defined as:

$$E_\xi(X) = \sum_{\rho=0}^{\infty} \frac{X^\rho}{\Gamma(\rho\xi + 1)}, \quad (6)$$

with ρ being a strictly positive constant. When two arguments are taken into account, the Mittag-Leffler function becomes

$$E_{\xi_1, \xi_2}(X) = \sum_{\rho=0}^{\infty} \frac{X^\rho}{\Gamma(\rho\xi_1 + \xi_2)}, \quad (7)$$

with $\xi_1, \xi_2 > 0$. Hence, one has $E_\xi(X) = E_{\xi,1}(X)$ and $E_{1,1}(X) = e^X$.

2.3 | Problem statement

Consider the following nonlinear system

$$\begin{cases} \dot{Z}_1 &= Z_2 \\ \dot{Z}_2 &= Z_3 \\ &\vdots \\ \dot{Z}_{n-1} &= Z_n \\ \dot{Z}_n &= F(Z) + G(Z)U + D(Z, t), \end{cases} \quad (8)$$

where the state vector is $Z = [Z_1, Z_2, \dots, Z_n]^T \in \mathbb{R}^n$ and the control input is $U \in \mathbb{R}$. Furthermore, $F(Z)$ and $G(Z) \neq 0$ are two known nonlinear functions, while $D(Z, t)$ represents uncertainties and external disturbances.

Assumption 1. It is assumed that $D(Z, t) < Y_T$ and $\dot{D}(Z, t) < Y_d$ where $Y_T > 0$ and $Y_d > 0$.

The control objective is to design a robust controller which guarantees FnT stability of the origin of the closed-loop system (8) without knowing the upper bound of the disturbances. The following lemmas will be useful to derive the main results.

Lemma 1 (¹²). Consider the sliding variable

$$S = \dot{Z}_n + \kappa_n \text{sign}(Z_n) |Z_n|^{\mu_n} + \dots + \kappa_1 \text{sign}(Z_1) |Z_1|^{\mu_1}, \quad (9)$$

where μ_j and κ_j ($j = 1, 2, \dots, n$) are positive constants such that the polynomial $p^n + \kappa_n p^{n-1} + \dots + \kappa_2 p + \kappa_1$ is Hurwitz and

$$\begin{cases} \mu_1 &= \mu, \\ \mu_{j-1} &= \frac{\mu_j \mu_{j+1}}{2\mu_{j+1} - \mu_j}, \quad j = 1, 2, \dots, n, \quad \forall n \geq 2 \end{cases} \quad (10)$$

with $\mu_{n+1} = 1$, $\mu_n = \mu$, $\mu \in (1 - \epsilon, 1)$ and $\epsilon \in (0, 1)$. Once the sliding mode is established (i.e., $S = 0$), the system state converges to zero in FnT.

Theorem 1. (Refer to Reference¹²) If the sliding-mode surface S is selected as (9) and the control is built as follows (11), the nonlinear system (8) will approach $S = 0$ in finite time and then converge to zero along $S = 0$ in FnT.

$$U = \frac{1}{G(Z)} (U_0 + U_1), \quad (11)$$

$$\mathcal{U}_0 = -\mathcal{F}(\mathcal{Z}) - \kappa_n \text{sign}(\mathcal{Z}_n) |\mathcal{Z}_n|^{\mu_n} - \dots - \kappa_1 \text{sign}(\mathcal{Z}_1) |\mathcal{Z}_1|^{\mu_1} \quad (12)$$

$$\begin{aligned} \dot{\mathcal{U}}_1 + \mathcal{T}\mathcal{U}_1 &= \zeta, \\ \zeta &= -(\Upsilon_d + \Upsilon_T + \zeta_0) \text{sign}(\sigma). \end{aligned} \quad (13)$$

where $\Upsilon_d, \Upsilon_T, \zeta$ are positive parameters. It has been proved that when $S = 0$, the system states converges to zero in finite time (referred to as t_s).

Lemma 2 ⁽¹⁷⁾. Consider the first-order nonlinear differential equation

$$\dot{\Upsilon} + \Lambda \text{sig}(\Upsilon)^\alpha = 0, \quad (14)$$

with $\Lambda > 0, 0 < \alpha < 1$. Then, Υ converges to zero in a finite-time given by

$$t_f = \frac{|\Upsilon(0)|^{1-\alpha}}{\Lambda(1-\alpha)}. \quad (15)$$

3 | THE PROPOSED FORITSM CONTROL LAW

To design the proposed robust controller, let us consider the following fractional-order integral terminal sliding variable, i.e.,

$$\sigma = S + \Lambda D^{\beta-1} S_I \quad (16)$$

with $\Lambda > 0, 0 < \beta < 1$. The sliding variable S is given in (9) and S_I can be designed as:

$$D^\beta S_I = \text{sign}(S) |S|^\alpha, \quad (17)$$

with initial value

$$S_I(0) = -\frac{1}{\Lambda} D^{1-\beta} S(0). \quad (18)$$

From Eqs. (16)-(18), one can easily see that $\sigma(0) = 0$. Hence, the reaching phase to the sliding surface $\sigma = 0$ is removed.

Remark 1. The proposed recursive form terminal sliding variable (16) combines two sliding variables (i.e., (9) and (17)). If an appropriate control input is designed such that the sliding mode is established (i.e., $\sigma = 0$), the system trajectories will be constrained to the sliding surface $\sigma = 0$, and then to the origin in FnT. Because of the integral initial condition in (18), the RP is cancelled in comparison to conventional TSM control. Moreover, compared to integral HOSM control, only two layers of sliding manifolds are adopted in the integral TSM, which is simpler for practical implementations. In addition, the proposed sliding manifold offers extract degree to increase the performance tracking of the full nonlinear system.

Compute now the time derivative of σ , i.e.,

$$\begin{aligned} \dot{\sigma} &= \dot{S} + \Lambda D^\beta S_{I\beta} \\ &= \ddot{\mathcal{Z}}_n + \kappa_n \mu_n |\mathcal{Z}_n|^{\mu_n-1} \dot{\mathcal{Z}}_n + \dots + \kappa_1 \mu_1 |\mathcal{Z}_1|^{\mu_1-1} \dot{\mathcal{Z}}_1 + \Lambda D^\beta S_{I\beta}. \end{aligned} \quad (19)$$

Theorem 2. Given the nonlinear system (8), consider the sliding variable (16) and the following controller

$$\mathcal{U} = \mathcal{G}(\mathcal{Z})^{-1} (\mathcal{U}_0 + \mathcal{U}_1) \quad (20)$$

$$\mathcal{U}_0 = -\mathcal{F}(\mathcal{Z}) - \kappa_n \text{sign}(\mathcal{Z}_n) |\mathcal{Z}_n|^{\mu_n} - \dots - \kappa_1 \text{sign}(\mathcal{Z}_1) |\mathcal{Z}_1|^{\mu_1} - \Lambda D^\beta S_I \quad (21)$$

$$D^\lambda \mathcal{U}_1 + \mathcal{T}\mathcal{U}_1 = \zeta_I,$$

$$\zeta_I = -(\Upsilon_d + \Upsilon_T + \zeta_0) D^{\lambda-1} \text{sign}(\sigma) - K_f D^{\lambda-1} \sigma, \quad (22)$$

with $\kappa_j > 0, \Upsilon_d, \Upsilon_T, \zeta_0$ being positive constants, λ being a fractional operator, and the two constants Υ_d and Υ_T chosen such that $\Upsilon_T > \mathcal{T}\delta$. Then, the trajectories of (8), constrained to $\sigma = 0$, will converge to zero in a FnT and the settling time satisfying $\mathcal{T}_{FnT} \leq t_s + t_s + t_c$.

Proof. Making reference to system (8), the sliding variable (16) can be expressed as

$$\begin{aligned} \sigma &= \dot{\mathcal{Z}}_n + \kappa_n \text{sign}(\mathcal{Z}_n) |\mathcal{Z}_n|^{\mu_n} + \dots + \kappa_1 \text{sign}(\mathcal{Z}_1) |\mathcal{Z}_1|^{\mu_1} + \Lambda D^{\beta-1} S_I \\ &= \mathcal{F}(\mathcal{Z}) + \mathcal{G}(\mathcal{Z})\mathcal{U} + D(\mathcal{Z}, t) + \kappa_n \text{sign}(\mathcal{Z}_n) |\mathcal{Z}_n|^{\mu_n} + \dots + \kappa_1 \text{sign}(\mathcal{Z}_1) |\mathcal{Z}_1|^{\mu_1} + \Lambda D^{\beta-1} S_I. \end{aligned} \quad (23)$$

Replacing the control (20) into equation (23) yields

$$\begin{aligned}\sigma &= \mathcal{F}(\mathcal{Z}) + \mathcal{U}_0 + \mathcal{U}_1 + \mathcal{D}(\mathcal{Z}) + \kappa_n \text{sign}(\mathcal{Z}_n) |\mathcal{Z}_n|^{\mu_n} + \dots + \kappa_1 \text{sign}(\mathcal{Z}_1) |\mathcal{Z}_1|^{\mu_1} + \Lambda \mathcal{D}^{\beta-1} \mathcal{S}_f \\ &= \mathcal{U}_1 + \mathcal{D}(\mathcal{Z}).\end{aligned}\quad (24)$$

The FO switching law can be written as

$$D^\lambda \mathcal{U}_1 + \mathcal{T} \mathcal{U}_1 = -(\Upsilon_d + \Upsilon_T + \zeta_0) D^{\lambda-1} \text{sign}(\sigma) - K_f D^{\lambda-1} \sigma \quad (25)$$

$$= -D^{\lambda-1} [(\Upsilon_d + \Upsilon_T + \zeta_0) \text{sign}(\sigma) - K_f \sigma]. \quad (26)$$

After simple calculation, one has

$$\dot{\mathcal{U}}_1 + \mathcal{T} D^{1-\lambda} \mathcal{U}_1 = - \underbrace{(\Upsilon_d + \Upsilon_T + \zeta_0) \text{sign}(\sigma) - K_f \sigma}_{\zeta_I}. \quad (27)$$

Since the Laplace transform of Eq. (27) is

$$s \mathcal{U}_1(s) - \mathcal{U}_1(0) + \mathcal{T} s^{1-\lambda} \mathcal{U}_1(s) - \mathcal{T} s^{-\lambda} \mathcal{U}_1(0) = \zeta_I(s), \quad (28)$$

with non negative constant $\mathcal{U}_1(0) = \mathcal{U}_1(0, \sigma(0))$, then Eq. (28) can be defined as

$$\mathcal{U}_1(s) = \frac{\zeta_I(s) s^{-1} + \mathcal{U}_1(0) s^{-1} + s^{-1-\lambda} \mathcal{U}_1(0)}{1 + \mathcal{T} s^{-\lambda}} \quad (29)$$

The unique solution of (29) arises from the uniqueness and existence theorem of fractional equations⁴² and the properties of inverse Laplace transform since $\mathcal{U}_1(t, \sigma)$ is locally Lipschitz with respect to σ . The solution of (25) is given by:

$$\mathcal{U}_1(t) = \mathcal{U}_1(0) t^{-\lambda} E_{-\lambda, -\lambda+1}(-\mathcal{T} t^{-\lambda}) + \mathcal{U}_1(0) E_{-\lambda}(-\mathcal{T} t^{-\lambda}) + \int_0^t (t-\tau)^{-\lambda} E_{-\lambda, -\lambda+1}(-\mathcal{T} (t-\tau)^{-\lambda}) \zeta_I(\tau) d\tau, \quad (30)$$

where $E_{-\lambda}(-\mathcal{T} t^\lambda)$ and $E_{-\lambda, -\lambda+1}(-\mathcal{T} t^\lambda)$ are Mittag-Leffler functions.

Using the condition $\Upsilon_T > \mathcal{T} \delta$ and from (24) and (30), under the condition $\mathcal{U}_1(0) = 0$, one obtains $\Upsilon_T \geq \mathcal{T}$, $\Upsilon_d \geq \mathcal{T}$, and $|\mathcal{U}_1|_{\max} \geq \mathcal{T} |\mathcal{U}_1(t)|$, which in turn implies $\mathcal{T} |\mathcal{U}_1(t)| \leq \Upsilon_T$. The fractional derivative of the terminal sliding manifold (24) is

$$D^\lambda \sigma = D^\lambda \mathcal{D}(\mathcal{Z}) + D^\lambda \mathcal{U}_1 \quad (31)$$

$$= D^\lambda \mathcal{D}(\mathcal{Z}) + D^\lambda \mathcal{U}_1 + \mathcal{T} \mathcal{U}_1 - \mathcal{T} \mathcal{U}_1 \quad (32)$$

$$= D^\lambda \mathcal{D}(\mathcal{Z}) + \zeta_I - \mathcal{T} \mathcal{U}_1 \quad (33)$$

$$= D^\lambda \mathcal{D}(\mathcal{Z}) - D^{\lambda-1} [(\Upsilon_d + \Upsilon_T + \zeta_0) \text{sign}(\sigma) - K_f \sigma] - \mathcal{T} \mathcal{U}_1. \quad (34)$$

Consider now the Lyapunov function and its time-derivative as $\mathcal{V} = \frac{1}{2} \sigma^2$ and $\dot{\mathcal{V}} = \sigma \dot{\sigma} = \sigma D^{1-\lambda} (D^\lambda \sigma)$. One gets

$$\dot{\mathcal{V}} = \sigma D^{1-\lambda} \{ D^\lambda \mathcal{D}(\mathcal{Z}) - D^{\lambda-1} [(\Upsilon_d + \Upsilon_T + \zeta_0) \text{sign}(\sigma) - K_f \sigma] - \mathcal{T} \mathcal{U}_1 \} \quad (35)$$

$$= \sigma \{ \dot{\mathcal{D}}(\mathcal{Z}) - [(\Upsilon_d + \Upsilon_T + \zeta_0) \text{sign}(\sigma) - K_f \sigma] - \mathcal{T} D^{1-\lambda} \mathcal{U}_1 \} \quad (36)$$

$$= \dot{\mathcal{D}}(\mathcal{Z}) \sigma - (\Upsilon_d + \Upsilon_T + \zeta_0) |\sigma| - K_f \sigma^2 - \mathcal{T} D^{1-\lambda} \mathcal{U}_1 \sigma \quad (37)$$

$$\leq |\dot{\mathcal{D}}(\mathcal{Z})| |\sigma| - \Upsilon_d |\sigma| + [-\mathcal{T} D^{1-\lambda} \mathcal{U}_1 \sigma - \Upsilon_T |\sigma|] - \zeta_0 |\sigma| - K_f \sigma^2 \quad (38)$$

According to the Assumption (1) and exploiting (35), one gets

$$\dot{\mathcal{V}} = \sigma \dot{\sigma} \leq -\zeta_0 |\sigma| - K_f \sigma^2. \quad (39)$$

To demonstrate the finite-time stability, (39) can be rewritten as

$$\dot{\mathcal{V}} \leq -2K_f \mathcal{V} - \sqrt{2\zeta_0} \mathcal{V}^{\frac{1}{2}}. \quad (40)$$

Dividing (40) by $\mathcal{V}^{\frac{1}{2}}$, one obtains

$$dt \leq - \frac{\mathcal{V}^{-\frac{1}{2}}}{2K_f \mathcal{V}^{\frac{1}{2}} + \sqrt{2\zeta_0}} d\mathcal{V}. \quad (41)$$

By integrating (41) from t_0 to t_c and after a simple calculation, it yields

$$t_c - t_0 \leq - \int_{\mathcal{V}(t_{x0})}^0 \frac{\mathcal{V}^{-\frac{1}{2}}}{2K_f \mathcal{V}^{\frac{1}{2}} + \sqrt{2}\zeta_0} d\mathcal{V} \quad (42)$$

$$= \frac{1}{K_f} \ln \frac{2K_f \mathcal{V}^{\frac{1}{2}}(t_{x0}) + \sqrt{2}\zeta_0}{\sqrt{2}\zeta_0}. \quad (43)$$

On the other hand, this implies that, in a finite amount of time, one has $\sigma = 0$, and the trajectories of system (8) will converge to zero in FnT as well, under $\sigma = 0$. In fact, if $\sigma = 0$ holds in (16), the sliding variable will converge to zero in a FnT according to Lemma 2, i.e.,

$$\begin{aligned} \sigma &= S + \Lambda D^{\beta-1} S_{I\beta} = 0 \\ D^\beta S_{I\beta} &= \text{sig}(S)^\alpha. \end{aligned} \quad (44)$$

Hence, one has

$$\begin{aligned} D^\beta S_{I\beta} &= \text{sig}(-\Lambda D^{\beta-1} S_{I\beta})^\alpha \\ &= -\Lambda^\alpha D^{\beta-1} \text{sig}^\alpha(S_{I\beta}), \end{aligned} \quad (45)$$

which, after a simple calculation, implies

$$\dot{S}_{I\beta} = -\Lambda^\alpha \text{sig}^\alpha(S_{I\beta}). \quad (46)$$

Making reference to Lemma 2, the convergence time t_s is given by

$$t_s = \frac{|\sigma(0)|^{1-\alpha}}{\Lambda(1-\alpha)}. \quad (47)$$

Finally, from Theorem 1 “ t_s ”, (43) and (46), the settling time can be estimated as $\mathcal{T}_{FnT} \leq t_s + t_s + t_c$. \square

Remark 2. The control signal (22) is the same as a fractional-order high-pass filter (FOHPF), with $\varepsilon(t)$ as the input and \mathcal{U}_1 as the filter’s output. The fractional-order filter’s Laplace transfer function (22) is given by

$$\frac{\mathcal{U}_1(t)}{\varepsilon(t)} = \frac{s^{\lambda-1}}{s^\lambda + \mathcal{T}}, \quad (48)$$

where \mathcal{T} is the FOHPF’s bandwidth, while $\mathcal{U}_1(t)$ in (20) is the output of the FOHPF (22) which is softened to be a smooth signal by the switch function, despite the fact that $\varepsilon(t)$ is non-smooth due to the switching function (22).

Remark 3. They are two advantages of the proposed of the fractional-order command filter compared to the integer-order command filter. First, for the recursive sliding manifold with given fractional order derivative and gain following the design guidelines. That is, the closed-loop system (8) could be finite-time stable with more degree of freedom. Second, the fundamental distinction between the proposed FO command filter and their integer filter, where it is shown that the parameter adds an extra degree of parameter degree of freedom. With the use of this parameter λ , the suggested technique may be able to better balance various conflict performance standards.

Remark 4. The disadvantage of the strategies proposed in^{9,12,10} is that the reaching phase is still present. The reaching phase is instead removed in our method due to the proposed recursive fractional-order integral terminal sliding manifold, and the system begins to move on the sliding surface since the initial time instant. Moreover, the proposal exhibits certain noteworthy characteristics with respect to existing methods in^{9,12,10}, which are outlined as follows:

- First, for the existing nonsingular terminal sliding manifold^{9,12,10}, the designed surface variables following the non-recursive manner can only admit an existence condition for FnT stability. Still, in the present paper, the proposed controller ensures finite-time stability without an existing condition and the settling time satisfying $\mathcal{T}_{FnT} \leq t_s + t_s + t_c$.
- It can be seen from the existing works^{12,17,45} that the proposed FORITSM offers two additional degrees of freedom, due to the designed FO filter and the FO cursive integral sliding manifold.

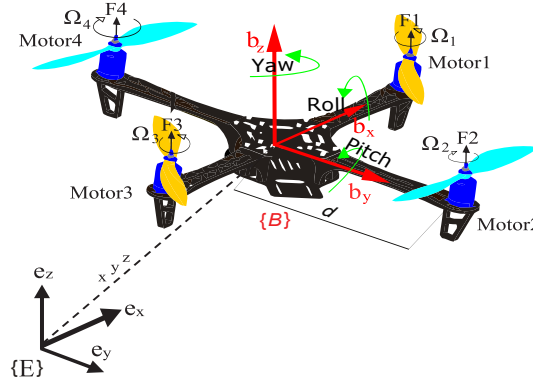


FIGURE 1 Quadrotor configuration.

4 | APPLICATION TO TRACKING CONTROL FOR A QUADROTOR UAV

In this section, the proposed control approach is applied to the dynamics of a quadrotor UAV, showing its applicability in a practical case.

4.1 | Modelling and tracking control problem

Consider a quadrotor system⁴⁶ captured by the following equations

$$\begin{aligned}
 \ddot{\phi} &= \dot{\theta}\dot{\psi}\frac{(J_{YY} - J_{ZZ})}{J_{XX}} - \frac{I_{rr}}{J_{XX}}\Omega_r\dot{\theta} - \frac{\partial\phi}{J_{XX}}\dot{\phi}^2 + \frac{1}{J_{XX}}\tau_\phi + D_\phi \\
 \ddot{\theta} &= \dot{\phi}\dot{\psi}\frac{(J_{ZZ} - J_{XX})}{J_{YY}} + \frac{I_{rr}}{J_{YY}}\Omega_r\dot{\phi} - \frac{\partial\theta}{J_{YY}}\dot{\theta}^2 + \frac{1}{J_{YY}}\tau_\theta + D_\theta \\
 \ddot{\psi} &= \dot{\phi}\dot{\theta}\frac{(J_{XX} - J_{YY})}{J_{ZZ}} - \frac{\partial\psi}{J_{ZZ}}\dot{\psi}^2 + \frac{1}{J_{ZZ}}\tau_\psi + D_\psi \\
 \ddot{x} &= -\frac{\partial_x}{m}\dot{x} + (\cos\phi\sin\theta\cos\psi + \sin\phi\sin\psi)\frac{T}{m} + D_x \\
 \ddot{y} &= -\frac{\partial_y}{m}\dot{y} + (\cos\phi\sin\theta\sin\psi - \sin\phi\cos\psi)\frac{T}{m} + D_y \\
 \ddot{z} &= -\frac{\partial_z}{m}\dot{z} - g + (\cos\phi\cos\theta)\frac{T}{m} + D_z,
 \end{aligned} \tag{49}$$

where the Euler angles of the quadrotor are expressed as $\Upsilon_\eta = [\phi \ \theta \ \psi]^T$, and $\dot{\Upsilon}_\eta = [\dot{\phi} \ \dot{\theta} \ \dot{\psi}]^T$ are the angular rates. As shown in Fig. (1), the absolute position of the the quadrotor is $\Upsilon_q = [x \ y \ z]^T$, and $\dot{\Upsilon}_q = [\dot{x} \ \dot{y} \ \dot{z}]^T$ represents the linear velocity, where J_{XX} , J_{YY} , and J_{ZZ} are inertia moments of the vehicle around b_x , b_y , b_z axes, m is the mass of the body, D_ϕ , D_θ , D_ψ , D_x , D_y and D_z denote the external disturbances, and g is the gravitational acceleration. Moreover, $\partial_i|_{x,y,z,\phi,\theta,\psi}$ are drag coefficients, and $[T \ \tau_\phi \ \tau_\theta \ \tau_\psi]^T$ are the control inputs. In order to generate the total thrust T and the tilting angles (ϕ_d, θ_d) , the virtual control input can be defined as follows

$$P_x = (\cos\phi\sin\theta\cos\psi + \sin\phi\sin\psi)\frac{T}{m} \tag{50}$$

$$P_y = (\cos\phi\sin\theta\sin\psi - \sin\phi\cos\psi)\frac{T}{m} \tag{51}$$

$$P_z = -g + (\cos\phi\cos\theta)\frac{T}{m}. \tag{52}$$

We are now in a position to formulate the considered tracking control problem. Specifically, the control objective is to design a FORITSM control for the system (49) in order to make the quadrotor follow a reference trajectory. In this context, the virtual signal $P_i = [P_x, P_y, P_z]^T$ will be designed in order to generate the total thrust T , the titling anglers (ϕ_d, θ_d) for the outer loop, and the torque controls $(\tau_\phi, \tau_\theta, \tau_\psi)$, as shown in Fig. (2).

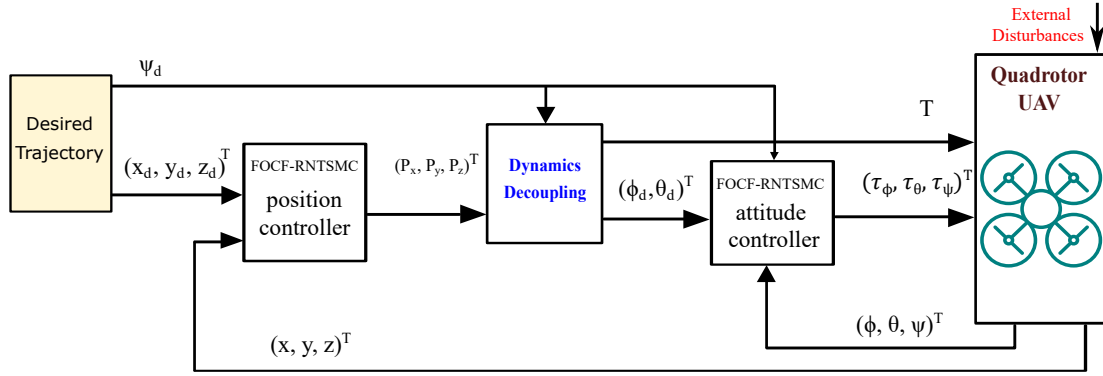


FIGURE 2 The proposed control scheme for the quadrotor UAV.

4.2 | FORITSM control design for the quadrotor

Let us define the tracking errors and their derivatives for the quadrotor position as follows

$$\mathbf{e}_x = x - x_d, \quad \dot{\mathbf{e}}_x = \dot{x} - \dot{x}_d, \quad \ddot{\mathbf{e}}_x = \ddot{x} - \ddot{x}_d \quad (53)$$

and

$$\mathbf{e}_y = y - y_d, \quad \dot{\mathbf{e}}_y = \dot{y} - \dot{y}_d, \quad \ddot{\mathbf{e}}_y = \ddot{y} - \ddot{y}_d \quad (54)$$

Similarly, the tracking errors and their derivatives are defined for the attitude as follows

$$\mathbf{e}_\phi = \phi - \phi_d, \quad \dot{\mathbf{e}}_\phi = \dot{\phi} - \dot{\phi}_d, \quad \ddot{\mathbf{e}}_\phi = \ddot{\phi} - \ddot{\phi}_d \quad (55)$$

and

$$\mathbf{e}_\theta = \theta - \theta_d, \quad \dot{\mathbf{e}}_\theta = \dot{\theta} - \dot{\theta}_d, \quad \ddot{\mathbf{e}}_\theta = \ddot{\theta} - \ddot{\theta}_d \quad (56)$$

Now, in order to design the proposed FORITSM control, the fast nonsingular terminal sliding manifolds for the position need to be defined as

$$S_x = \ddot{\mathbf{e}}_x + \kappa_{2x} \text{sign}(\dot{\mathbf{e}}_x) |\dot{\mathbf{e}}_x|^{\mu_{x2}} + \kappa_{x1} \text{sign}(\mathbf{e}_x) |\mathbf{e}_x|^{\mu_{x1}} \quad (57)$$

$$S_y = \ddot{\mathbf{e}}_y + \kappa_{2y} \text{sign}(\dot{\mathbf{e}}_y) |\dot{\mathbf{e}}_y|^{\mu_{y2}} + \kappa_{y1} \text{sign}(\mathbf{e}_y) |\mathbf{e}_y|^{\mu_{y1}} \quad (58)$$

$$S_z = \ddot{\mathbf{e}}_z + \kappa_{2z} \text{sign}(\dot{\mathbf{e}}_z) |\dot{\mathbf{e}}_z|^{\mu_{z2}} + \kappa_{z1} \text{sign}(\mathbf{e}_z) |\mathbf{e}_z|^{\mu_{z1}}. \quad (59)$$

The fast nonsingular terminal sliding manifolds for the attitude are instead given by

$$S_\phi = \ddot{\mathbf{e}}_\phi + \kappa_{2\phi} \text{sign}(\dot{\mathbf{e}}_\phi) |\dot{\mathbf{e}}_\phi|^{\mu_{\phi2}} + \kappa_{\phi1} \text{sign}(\mathbf{e}_\phi) |\mathbf{e}_\phi|^{\mu_{\phi1}} \quad (60)$$

$$S_\theta = \ddot{\mathbf{e}}_\theta + \kappa_{2\theta} \text{sign}(\dot{\mathbf{e}}_\theta) |\dot{\mathbf{e}}_\theta|^{\mu_{\theta2}} + \kappa_{\theta1} \text{sign}(\mathbf{e}_\theta) |\mathbf{e}_\theta|^{\mu_{\theta1}} \quad (61)$$

$$S_\psi = \ddot{\mathbf{e}}_\psi + \kappa_{2\psi} \text{sign}(\dot{\mathbf{e}}_\psi) |\dot{\mathbf{e}}_\psi|^{\mu_{\psi2}} + \kappa_{\psi1} \text{sign}(\mathbf{e}_\psi) |\mathbf{e}_\psi|^{\mu_{\psi1}}. \quad (62)$$

The control parameters μ_{i1} and μ_{i2} for $(i = x, y, z, \phi, \theta, \psi)$ are selected according to Lemma 1, while κ_{i1} and κ_{i2} are positive coefficients.

The fractional-order integral terminal sliding manifolds for the position and attitude are respectively

$$\sigma_x = S_x + \Lambda_x D^{\beta_x - 1} S_{I\beta_x}, \quad \sigma_y = S_y + \Lambda_y D^{\beta_y - 1} S_{I\beta_y}, \quad \sigma_z = S_z + \Lambda_z D^{\beta_z - 1} S_{I\beta_z}, \quad (63)$$

and

$$\sigma_\phi = S_\phi + \Lambda_\phi D^{\beta_\phi - 1} S_{I\beta_\phi}, \quad \sigma_\theta = S_\theta + \Lambda_\theta D^{\beta_\theta - 1} S_{I\beta_\theta}, \quad \sigma_\psi = S_\psi + \Lambda_\psi D^{\beta_\psi - 1} S_{I\beta_\psi}, \quad (64)$$

where Λ_i are positive coefficients and S_i as in (57) and (62), while $S_{I\beta_i}$ can be designed as

$$D^{\beta_x} S_{I\beta_x} = \text{sig}(S_x)^{\alpha_x}, \quad D^{\beta_y} S_{I\beta_y} = \text{sig}(S_y)^{\alpha_y}, \quad D^{\beta_z} S_{I\beta_z} = \text{sig}(S_z)^{\alpha_z}, \quad (65)$$

and

$$D^{\beta_\phi} S_{I\beta_\phi} = \text{sig}(S_\phi)^{\alpha_\phi}, \quad D^{\beta_\theta} S_{I\beta_\theta} = \text{sig}(S_\theta)^{\alpha_\theta}, \quad D^{\beta_\psi} S_{I\beta_\psi} = \text{sig}(S_\psi)^{\alpha_\psi}. \quad (66)$$

Assumption 2. We assume the disturbance D_i is bounded and its derivative \dot{D}_i is also bounded. Both disturbance and its derivative satisfy the following conditions : $|D_i| < Y_{Ti}$ and $|\dot{D}_i| < Y_{di}$. Keep in mind that this assumption holds true in real-world scenarios. As an illustration, the load torque may hang when a cutting tool or end mill of a CNC machine tool cuts a work-piece as the cutting thickness increases, but the change rate of the load torque is always constrained.

Theorem 3. Given the quadrotor dynamics (49), controlled via the FORITSM control laws (67)-(84), that is, for the x -subsystem

$$P_x = (P_{x0} + P_{x1}) \quad (67)$$

$$P_{x0} = -\frac{\partial_x}{m}\dot{x} - \kappa_{2x}\text{sign}(\dot{\mathbf{e}}_x) |\dot{\mathbf{e}}_x|^{\mu_{x2}} - \kappa_{x1}\text{sign}(\mathbf{e}_x) |\mathbf{e}_x|^{\mu_{x1}} - \Lambda_x D^{\beta_x} S_{I\beta_x} \quad (68)$$

$$\begin{aligned} D^{\lambda_x} P_{x1} + \mathcal{T}_x P_{x1} &= \zeta_x, \\ \zeta_x &= -(\Upsilon_{dx} + \Upsilon_{Tx} + \zeta_{x0}) D^{\lambda_x-1} \text{sign}(\sigma_x) - K_{fx} D^{\lambda_x-1} \sigma_x, \end{aligned} \quad (69)$$

for the y -subsystem

$$P_y = (P_{y0} + P_{y1}) \quad (70)$$

$$P_{y0} = -\frac{\partial_y}{m}\dot{y} - \kappa_{2y}\text{sign}(\dot{\mathbf{e}}_y) |\dot{\mathbf{e}}_y|^{\mu_{y2}} - \kappa_{y1}\text{sign}(\mathbf{e}_y) |\mathbf{e}_y|^{\mu_{y1}} - \Lambda_y D^{\beta_y} S_{I\beta_y} \quad (71)$$

$$\begin{aligned} D^{\lambda_y} P_{y1} + \mathcal{T}_y P_{y1} &= \zeta_y, \\ \zeta_y &= -(\Upsilon_{dy} + \Upsilon_{Ty} + \zeta_{y0}) D^{\lambda_y-1} \text{sign}(\sigma_y) - K_{fy} D^{\lambda_y-1} \sigma_y, \end{aligned} \quad (72)$$

for the z -subsystem

$$P_z = (P_{z0} + P_{z1}) \quad (73)$$

$$P_{z0} = -\frac{\partial_z}{m}\dot{z} + g - \kappa_{2z}\text{sign}(\dot{\mathbf{e}}_z) |\dot{\mathbf{e}}_z|^{\mu_{z2}} - \kappa_{z1}\text{sign}(\mathbf{e}_z) |\mathbf{e}_z|^{\mu_{z1}} - \Lambda_z D^{\beta_z} S_{I\beta_z} \quad (74)$$

$$\begin{aligned} D^{\lambda_z} P_{z1} + \mathcal{T}_z P_{z1} &= \zeta_z, \\ \zeta_z &= -(\Upsilon_{dz} + \Upsilon_{Tz} + \zeta_{z0}) D^{\lambda_z-1} \text{sign}(\sigma_z) - K_{fz} D^{\lambda_z-1} \sigma_z, \end{aligned} \quad (75)$$

for the ϕ -subsystem

$$\tau_\phi = J_{XX} (\tau_{\phi0} + \tau_{\phi1}) \quad (76)$$

$$\tau_{\phi0} = -\left\{ \dot{\theta}\dot{\psi} \frac{(J_{YY} - J_{ZZ})}{J_{XX}} - \frac{I_{rr}}{J_{XX}} \Omega_r \dot{\theta} - \frac{\partial_\phi}{J_{XX}} \dot{\phi}^2 \right\} - \kappa_{2\phi}\text{sign}(\dot{\mathbf{e}}_\phi) |\dot{\mathbf{e}}_\phi|^{\mu_{\phi2}} - \kappa_{\phi1}\text{sign}(\mathbf{e}_\phi) |\mathbf{e}_\phi|^{\mu_{\phi1}} - \Lambda_\phi D^{\beta_\phi} S_{I\beta_\phi} \quad (77)$$

$$\begin{aligned} D^{\lambda_\phi} \tau_{\phi1} + \mathcal{T}_\phi \tau_{\phi1} &= \zeta_\phi, \\ \zeta_\phi &= -(\Upsilon_{d\phi} + \Upsilon_{T\phi} + \zeta_{\phi0}) D^{\lambda_\phi-1} \text{sign}(\sigma_\phi) - K_{f\phi} D^{\lambda_\phi-1} \sigma_\phi, \end{aligned} \quad (78)$$

for the θ -subsystem

$$\tau_\theta = J_{YY} (\tau_{\theta0} + \tau_{\theta1}) \quad (79)$$

$$\tau_{\theta0} = -\left\{ \dot{\phi}\dot{\psi} \frac{(J_{ZZ} - J_{XX})}{J_{YY}} + \frac{I_{rr}}{J_{YY}} \Omega_r \dot{\phi} - \frac{\partial_\theta}{J_{YY}} \dot{\theta}^2 \right\} - \kappa_{2\theta}\text{sign}(\dot{\mathbf{e}}_\theta) |\dot{\mathbf{e}}_\theta|^{\mu_{\theta2}} - \kappa_{\theta1}\text{sign}(\mathbf{e}_\theta) |\mathbf{e}_\theta|^{\mu_{\theta1}} - \Lambda_\theta D^{\beta_\theta} S_{I\beta_\theta} \quad (80)$$

$$\begin{aligned} D^{\lambda_\theta} \tau_{\theta1} + \mathcal{T}_\theta \tau_{\theta1} &= \zeta_\theta, \\ \zeta_\theta &= -(\Upsilon_{d\theta} + \Upsilon_{T\theta} + \zeta_{\theta0}) D^{\lambda_\theta-1} \text{sign}(\sigma_\theta) - K_{f\theta} D^{\lambda_\theta-1} \sigma_\theta, \end{aligned} \quad (81)$$

and for the ψ -subsystem

$$\tau_\psi = J_{ZZ} (\tau_{\psi0} + \tau_{\psi1}) \quad (82)$$

$$\tau_{\psi0} = -\left\{ \dot{\phi}\dot{\psi} \frac{(J_{XX} - J_{YY})}{J_{ZZ}} - \frac{\partial_\psi}{J_{ZZ}} \dot{\psi}^2 \right\} - \kappa_{2\psi}\text{sign}(\dot{\mathbf{e}}_\psi) |\dot{\mathbf{e}}_\psi|^{\mu_{\psi2}} - \kappa_{\psi1}\text{sign}(\mathbf{e}_\psi) |\mathbf{e}_\psi|^{\mu_{\psi1}} - \Lambda_\psi D^{\beta_\psi} S_{I\beta_\psi} \quad (83)$$

$$\begin{aligned} D^{\lambda_\psi} \tau_{\psi1} + \mathcal{T}_\psi \tau_{\psi1} &= \zeta_\psi, \\ \zeta_\psi &= -(\Upsilon_{d\psi} + \Upsilon_{T\psi} + \zeta_{\psi0}) D^{\lambda_\psi-1} \text{sign}(\sigma_\psi) - K_{f\psi} D^{\lambda_\psi-1} \sigma_\psi, \end{aligned} \quad (84)$$

where $\kappa_{i1}, \kappa_{i2} > 0$, Υ_{di} , Υ_{Ti} , and ζ_{0i} are positive constants, λ_i is fractional operator, and Υ_{di} and Υ_{Ti} are two constants, if $\Upsilon_{Ti} > \mathcal{T}_i \delta_i$, then $\sigma_x, \sigma_y, \sigma_z, \sigma_\phi, \sigma_\theta$, and σ_ψ are zeroed in a finite time. Moreover, the position and attitude dynamics in (49) are

regulated to their references in a finite time, constrained to the sliding mode on $\sigma_x = \sigma_y = \sigma_z = \sigma_\phi = \sigma_\theta = \sigma_\psi = 0$. **The global settling time for quadrotor position and attitude satisfying $T_{GFnT} \leq T_{xFnT} + T_{yFnT} + T_{zFnT} + T_{\phi FnT} + T_{\theta FnT} + T_{\psi FnT}$.**

Proof. Taking into account the sliding manifolds in (57), (62), and substituting the proposed control laws (67)-(84) to (63), (64), one has

$$\sigma_x = P_{x1} + D_x, \quad \sigma_y = P_{y1} + D_y, \quad \sigma_z = P_{z1} + D_z, \quad (85)$$

and

$$\sigma_\phi = \tau_{\phi 1} + D_\phi, \quad \sigma_\theta = \tau_{\theta 1} + D_\theta, \quad \sigma_\psi = \tau_{\psi 1} + D_\psi. \quad (86)$$

Using the results of the Theorem 2, the solutions of the control inputs (69), (72), (75), (78), (81), and (84) are

$$P_{y1}(t) = P_{x1}(0)t^{-\lambda_x} E_{-\lambda_x, -\lambda_x+1}(-\mathcal{T}_x t^{-\lambda_x}) + P_{x1}(0)E_{-\lambda_x}(-\mathcal{T}_x t^{-\lambda_x}) + \int_0^t (t-\tau)^{-\lambda_x} E_{-\lambda_x, -\lambda_x+1}(-\mathcal{T}_x(t-\tau)^{-\lambda_x}) \zeta_x(\tau) d\tau \quad (87)$$

$$P_{y1}(t) = P_{y1}(0)t^{-\lambda_y} E_{-\lambda_y, -\lambda_y+1}(-\mathcal{T}_y t^{-\lambda_y}) + P_{x1}(0)E_{-\lambda_y}(-\mathcal{T}_y t^{-\lambda_y}) + \int_0^t (t-\tau)^{-\lambda_y} E_{-\lambda_y, -\lambda_y+1}(-\mathcal{T}_y(t-\tau)^{-\lambda_y}) \zeta_y(\tau) d\tau \quad (88)$$

$$P_{z1}(t) = P_{z1}(0)t^{-\lambda_z} E_{-\lambda_z, -\lambda_z+1}(-\mathcal{T}_z t^{-\lambda_z}) + P_{x1}(0)E_{-\lambda_z}(-\mathcal{T}_z t^{-\lambda_z}) + \int_0^t (t-\tau)^{-\lambda_z} E_{-\lambda_z, -\lambda_z+1}(-\mathcal{T}_z(t-\tau)^{-\lambda_z}) \zeta_z(\tau) d\tau \quad (89)$$

$$\tau_{\phi 1}(t) = \tau_{\phi 1}(0)t^{-\lambda_\phi} E_{-\lambda_\phi, -\lambda_\phi+1}(-\mathcal{T}_\phi t^{-\lambda_\phi}) + P_{x1}(0)E_{-\lambda_\phi}(-\mathcal{T}_\phi t^{-\lambda_\phi}) + \int_0^t (t-\tau)^{-\lambda_\phi} E_{-\lambda_\phi, -\lambda_\phi+1}(-\mathcal{T}_\phi(t-\tau)^{-\lambda_\phi}) \zeta_\phi(\tau) d\tau \quad (90)$$

$$\tau_{\theta 1}(t) = \tau_{\theta 1}(0)t^{-\lambda_\theta} E_{-\lambda_\theta, -\lambda_\theta+1}(-\mathcal{T}_\theta t^{-\lambda_\theta}) + P_{x1}(0)E_{-\lambda_\theta}(-\mathcal{T}_\theta t^{-\lambda_\theta}) + \int_0^t (t-\tau)^{-\lambda_\theta} E_{-\lambda_\theta, -\lambda_\theta+1}(-\mathcal{T}_\theta(t-\tau)^{-\lambda_\theta}) \zeta_\theta(\tau) d\tau \quad (91)$$

$$\tau_{\psi 1}(t) = \tau_{\psi 1}(0)t^{-\lambda_\psi} E_{-\lambda_\psi, -\lambda_\psi+1}(-\mathcal{T}_\psi t^{-\lambda_\psi}) + P_{x1}(0)E_{-\lambda_\psi}(-\mathcal{T}_\psi t^{-\lambda_\psi}) + \int_0^t (t-\tau)^{-\lambda_\psi} E_{-\lambda_\psi, -\lambda_\psi+1}(-\mathcal{T}_\psi(t-\tau)^{-\lambda_\psi}) \zeta_\psi(\tau) d\tau \quad (92)$$

Using the condition $\Upsilon_{Ti} > \mathcal{T}_i \delta_i$ and from (24) and (87)-(92), under the condition $P_x(0) = P_y(0) = P_z(0) = \tau_\phi(0) = \tau_\theta(0) = \tau_\psi = 0$ one obtains $\Upsilon_{Ti} \geq \mathcal{T}_i$, $\Upsilon_{di} \geq \mathcal{T}_i \left| P_{x1}, P_{y1}, P_{z1}, \tau_{\phi 1}, \tau_{\theta 1}, \tau_{\psi 1} \right|_{\max} \geq \mathcal{T}_i \left| P_{x1}, P_{y1}, P_{z1}, \tau_{\phi 1}, \tau_{\theta 1}, \tau_{\psi 1} \right|$, i.e., $\mathcal{T}_i \left| P_{x1}, P_{y1}, P_{z1}, \tau_{\phi 1}, \tau_{\theta 1}, \tau_{\psi 1} \right| \leq \Upsilon_{Ti}$.

Consider now the global Lyapunov function for overall quadrotor system $\mathcal{V}_g = \frac{1}{2} \left[\sigma_x^2 + \sigma_y^2 + \sigma_z^2 + \sigma_\phi^2 + \sigma_\theta^2 + \sigma_\psi^2 \right]$. The FO derivative of terminal sliding manifold is

$$D^{\lambda_i} \sigma_i = D^{\lambda_i} \mathcal{D}_i + D^{\lambda_i} \Gamma \quad (93)$$

$$= D^{\lambda_i} \mathcal{D}_i + D_i^{\lambda_i} \Gamma + \mathcal{T}_i \Gamma - \mathcal{T}_i \Gamma \quad (94)$$

$$= D^{\lambda_i} \mathcal{D}_i + \zeta_i - \mathcal{T}_i \Gamma \quad (95)$$

$$= D^{\lambda_i} \mathcal{D}_i - D^{\lambda_i-1} \left[(\Upsilon_{di} + \Upsilon_{Ti} + \zeta_{0i}) \text{sign}(\sigma_i) - K_{fi} \sigma_i \right] - \mathcal{T}_i \Gamma. \quad (96)$$

with Γ representing the input controls $P_x, P_y, P_z, \tau_\phi, \tau_\theta, \tau_\psi$. Hence,

$$\sigma_i \dot{\sigma}_i = \dot{\mathcal{D}}_i \sigma_i - (\Upsilon_{di} + \Upsilon_{Ti} + \zeta_{0i}) |\sigma_i| - K_{fi} \sigma_i^2 - \mathcal{T}_i D^{1-\lambda_i} \Gamma \sigma_i \quad (97)$$

$$\leq |\dot{\mathcal{D}}_i| |\sigma_i| - \Upsilon_{di} |\sigma_i| + [-\mathcal{T}_i D^{1-\lambda_i} \Gamma \sigma_i - \Upsilon_{Ti} |\sigma_i|] - \zeta_{0i} |\sigma_i| - K_{fi} \sigma_i^2 \quad (98)$$

According to Assumption (2) and exploiting (97), one has

$$\dot{\mathcal{V}}_g = \sigma_x \dot{\sigma}_x + \sigma_y \dot{\sigma}_y + \sigma_z \dot{\sigma}_z + \sigma_\phi \dot{\sigma}_\phi + \sigma_\theta \dot{\sigma}_\theta + \sigma_\psi \dot{\sigma}_\psi \quad (99)$$

$$\leq -\left(\sum_{i=x,y,z,\phi,\theta,\psi} \varsigma_{0i} |\sigma_i| + K_{fi} \sigma_i^2 \right) < 0. \quad (100)$$

From (99), we can conclude that the finite-time stability is established for the quadrotor system then, the settling time satisfies $t_{Gc} \leq t_{xc} + t_{yc} + t_{zc} + t_{\phi c} + t_{\theta c} + t_{\psi c}$. Furthermore, it has been verified that the sliding variable $\sigma_i = 0$ and then the tracking error e_i will converge to zero along the sliding surfaces $\sigma_i = 0$ and S_i successively in the finite time under the times t_{is} and t_{iS} . This one is based on the results of Theorem 2. However, the quadrotor system has six settling times one, i.e. $t_{Gs} \leq t_{xs} + t_{ys} + t_{zs} + t_{\phi s} + t_{\theta s} + t_{\psi s}$ and $t_{iS} \leq t_{xS} + t_{yS} + t_{zS} + t_{\phi S} + t_{\theta S} + t_{\psi S}$. As well as the quadrotor system trajectories will converge to zero in FnT. Finally, we demonstrate the finite-time stability of the quadrotor system and convergence time of its system, also the global setting time satisfies $T_{GFnT} \leq T_{xFnT} + T_{yFnT} + T_{zFnT} + T_{\phi FnT} + T_{\theta FnT} + T_{\psi FnT}$. \square

5 | SIMULATION RESULTS

In this section, realistic simulation results are illustrated to assess the proposed control approach, even in comparison with the control law proposed in ¹².

Remark 5. The smoothness of thrust and torques of the vehicle, external disturbances and other factors can really have an impact on the position and attitude desired control performances. To strike a balance between the trade-offs of control precision, energy consumption, and signal smoothness, suitable values for the control parameters should be chosen. Due to these factors, Simulation 1 (without disturbances) uses the toolbox of optimization in the MATLAB software to choose the optimal values for the controller parameters, and the remaining scenarios use the same parameters (see Ref. ⁴⁷).

From (15), the parameters of Λ and α in (15) directly influence on the control performance. t_f is more sensitive to of the parameter Λ than to α variations in the parameter.

5.1 | Settings

In the following a wide simulation campaign is discussed. More specifically, the following scenarios are considered:

Nominal model: In this scenario the proposed FORITSM control for position tracking is considered by using nominal parameters of the quadrotor. In addition, the simulation results of the proposed controller are compared with those achieve by using the control law in ¹².

Increasing disturbance amplitudes: In this scenario the proposed controller and the controller proposed in ¹² are tested considering the disturbances in (101) and (102) applied respectively for position and attitude of the quadrotor, by increasing their amplitudes with respect to time:

$$\begin{aligned} D_x &= \sin(4t) + \cos(4t), \quad t \in [0, \pi] \\ D_x &= 1.3 \sin(4t) + 1.3 \cos(4t), \quad t \in]\pi, 80] \\ D_y &= \sin(5t) + \cos(5t), \quad t \in [0, \frac{5}{7}\pi] \\ D_y &= 1.1 \sin(5t) + 1.4 \cos(5t), \quad t \in]\frac{5}{7}\pi, 80] \\ D_z &= \sin(5t) + \cos(5t), \quad t \in [0, 2\pi] \\ D_z &= 2 \sin(4t) + 2 \cos(5t), \quad t \in]2\pi, 80] \end{aligned} \quad (101)$$

and

$$\begin{aligned}
 D_\phi &= 1.3 \sin(5t) + 1.3 \cos(5t), \quad t \in [0, 2\pi] \\
 D_\phi &= 4 \sin(5t) + 4 \cos(5t), \quad t \in]2\pi, 8\pi] \\
 D_\theta &= 1.6 \sin(5t) + 1.6 \cos(5t), \quad t \in [0, 2\pi] \\
 D_\theta &= 4 \sin(5t) + 4 \cos(5t), \quad t \in]2\pi, 8\pi] \\
 D_\phi &= 1.5 \sin(5t) + 2 \cos(5t), \quad t \in [0, 2\pi] \\
 D_\phi &= 5 \sin(4t) + 5 \cos(5t), \quad t \in]2\pi, 8\pi].
 \end{aligned} \tag{102}$$

Increasing disturbance frequencies: In this scenario the proposed control method and the controller proposed in¹² are tested considering the disturbances in (103) and (104) applied respectively for position and attitude of the quadrotor, by increasing their frequencies with respect to time.

$$\begin{aligned}
 D_x &= \sin(4t) + \cos(4t), \quad t \in [0, \pi] \\
 D_x &= \sin(40t) + \cos(40t), \quad t \in]\pi, 8\pi] \\
 D_y &= \sin(5t) + \cos(5t), \quad t \in [0, \frac{5}{7}\pi] \\
 D_y &= \sin(50t) + \cos(50t), \quad t \in]\frac{5}{7}\pi, 8\pi] \\
 D_z &= \sin(5t) + \cos(5t), \quad t \in [0, 2\pi] \\
 D_z &= \sin(100t) + \cos(100t), \quad t \in]2\pi, 8\pi]
 \end{aligned} \tag{103}$$

and

$$\begin{aligned}
 D_\phi &= 3 \sin(5t) + 3 \cos(5t), \quad t \in [0, 2\pi] \\
 D_\phi &= \sin(100t) + \cos(100t), \quad t \in]2\pi, 8\pi] \\
 D_\theta &= 1.6 \sin(5t) + 1.6 \cos(5t), \quad t \in [0, 2\pi] \\
 D_\theta &= 1.6 \sin(5t) + 1.6 \cos(5t), \quad t \in]2\pi, 8\pi] \\
 D_\psi &= 5 \sin(100t) + 2 \cos(100t), \quad t \in [0, 2\pi] \\
 D_\psi &= \sin(100t) + \cos(100t), \quad t \in]2\pi, 8\pi]
 \end{aligned} \tag{104}$$

TABLE 1 Quadrotor parameters.

Parameter	Value	Parameter	Value
$g(s^{-2}.m)$	9.8	ϑ_y (Nms ²)	0.01
$m(kg)$	0.486	ϑ_z (Nms ²)	0.01
$J_{XX}(m^{-2}.kg)$	3.8278e-3	ϑ_ϕ (Nrad s ²)	0.012
$J_{YY}(m^{-2}.kg)$	3.8278e-3	ϑ_θ (Nrad s ²)	0.012
$J_{ZZ}(m^{-2}.kg)$	7.6566e-3	ϑ_ψ (Nrad s ²)	0.012
$I_{rr}(m^{-2}.kg)$	2.8385e-5	$b_N(N.s^2)$	2.9842e-3
ϑ_x (Nms ²)	0.01	$c_d(N.m.s^2)$	3.2320e-2

The quadrotor parameters for the considered scenarios are reported in Table 1, while the control parameters are given by $\mu_{i1} = \frac{9}{16}$, $\mu_{i2} = \frac{9}{23}$, $\alpha_{i1} = 0.2$, $\beta_{i2} = 72$, $\Lambda_1 = 0.05$, $\epsilon_{0i} = 0.5$, $\kappa_{2i} = 72$, $\kappa_{1i} = 192$, $\Upsilon_{di} = 14$, and $\Upsilon_{Ti} = 2.4$.

5.2 | Nominal model

Now the first scenario in nominal conditions is discussed. Fig. 3 shows the reference position tracking results. It can be observed that, by using the proposed method, fast and precise trajectory tracking is achieved, differently from the case when the method proposed in¹² is adopted. Indeed, the latter determines a big overshoot in the position outputs. The tracking performance of the attitude is instead plotted in Fig. 4, with satisfactory results when using the proposal. The tracking errors including e_x , e_y , e_z , and e_ψ are zeroed as expected and displayed in Fig. 5. The results of the tracking in 2D and 3D environments are plotted respectively in Fig. 6 and Fig. 7. Fig. 8 finally shows the results of the control inputs whose amplitudes are small and converge to their nominal values. **The input results of both proposed controller and the controller proposed in¹² are similar in this case. Moreover, the next scenario we increasing disturbance amplitudes in the quadrotor system.**

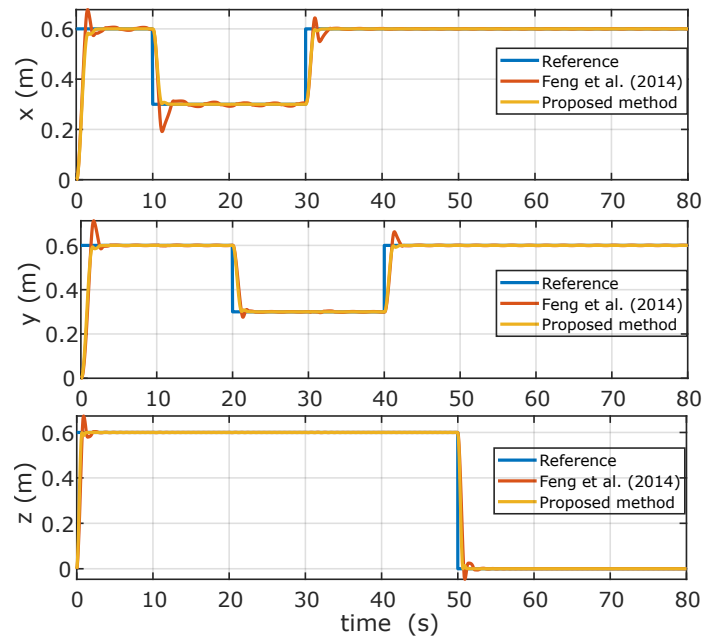


FIGURE 3 Simulation results showing the position performance of each controller: reference (—), control in Feng et al. (2014) (—), and proposed method (—) (Nominal model).

5.3 | Increasing disturbance amplitudes

To show the improvement obtained by the proposed controller, a comparative study with three nonlinear controllers is considered in this case. The existing controllers are proposed by the authors Feng et al.¹², Shi et al. (2019)⁴⁸, and Labbadi et al.⁴⁹. The results of the second scenario are now discussed with other three controllers. It can be seen that the proposed controller drives the outputs to converge to their desired trajectories in FnT. Moreover, the negative effect caused by the presence of the disturbances is removed. On the other hand, it can be noticed that the results provided by the control laws in¹²,⁴⁸, and⁴⁹ are less satisfactory than the ones achieved via the proposed method, see, for example, Fig. 9 where high oscillation are present. The attitude and tracking errors are plotted respectively in Fig. 10 and 11. Again, it can be observed that the attitude and tracking errors are zeroed. Finally, Figs. 12 and 13 of three controllers show that the proposed controller allows to achieve a good tracking performance compared to¹²,⁴⁸, and⁴⁹. The amplitudes of the inputs presented in Fig. 14 are small and with a reduced chattering phenomenon of both proposed controller and the approach proposed in¹². Indeed, the input results⁴⁸, and⁴⁹ are not small and with high amplitudes.

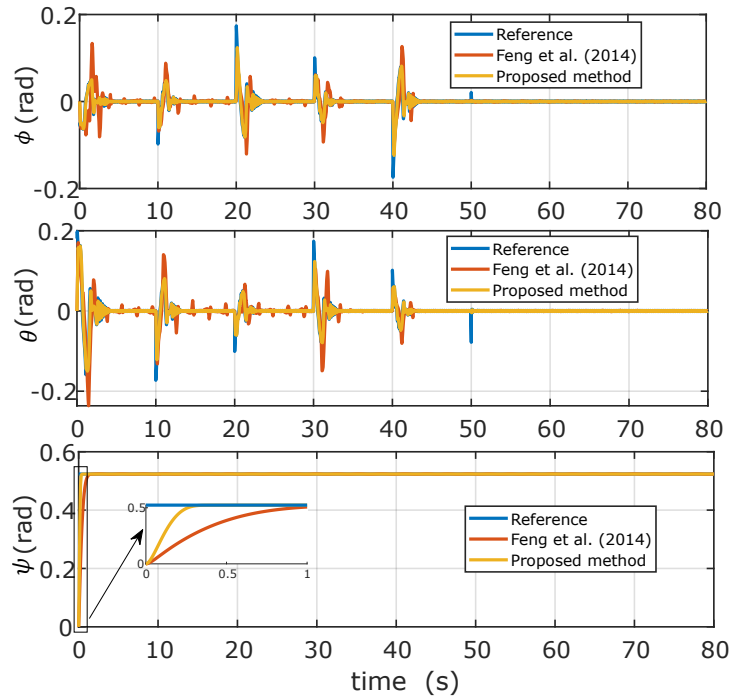


FIGURE 4 Simulation results showing the attitude performance of each controller: reference (—), control in Feng et al. (2014) (—), and proposed method (—) (Nominal model).

5.4 | Increasing disturbance frequencies

The results of the third scenario are illustrated hereafter. In terms of the convergence rate, rejection of the disturbances, and tracking performance, the proposed controller outperforms the one in¹² as shown in Figs. 15 and 16 for position and attitude respectively, as well as in terms of tracking errors. In fact, the proposed approach ensures fast convergence rate with lower undershoot of the system-controlled outputs. Indeed, the tracking performance of the 2D and 3D trajectories are displayed in Figs. 18 and 19. On the other hand, the proposed method generates continuous control signals as displayed in Fig. 20, which reduces chattering and improves the closed-loop system tracking control performance.

Remark 6. The results in Fig. 20 demonstrate that the type of disturbances that can impact the quadrotor system determines the algorithm that gives a lower upper bound of switching controller, as a result, a lower chattering amplitude. This is because this technique addresses the disturbance directly, but the proposed strategy addresses the disturbance's derivative.

Remark 7. The proposed controller has two parts. The first part is based on two layers of sliding mode variables with one FO operator. The second term of the proposed controller is based on FO switching controller. This makes the proposed controller more robust against the change of the frequencies of the disturbances due to the use of fractional-order operators in its design. In another hand, the proposed controller used switching gains to make it more robust against the change of the amplitude disturbances.

5.5 | Quantitative analysis of the controllers

This section will qualitatively assess the benefit of the proposed controller in reducing the impact of the rate limit. The closed-loop system, which exhibits system stability, has a potential for infinite loops, which are the main focus of the analysis. For quantitative comparison, the integral of the square value of the error (ISE), $\int_{t_i}^{t_f} e^2 dt$, is utilized. A numerical illustration of tracking-error performance is the ISE. For situations 2 “Increasing disturbance amplitudes”, the ISE performance of four controllers is displayed in Table 2. The proposed control strategy demonstrates that the ISE indices are less significant than the

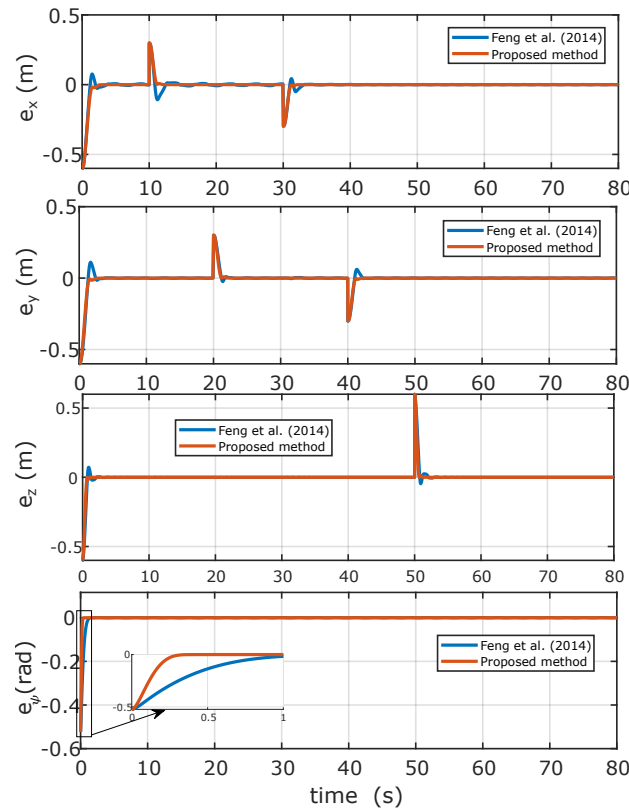


FIGURE 5 Simulation results showing the tracking errors performance of each controller: control in Feng et al. (2014) (—) and proposed method (—) (Nominal model).

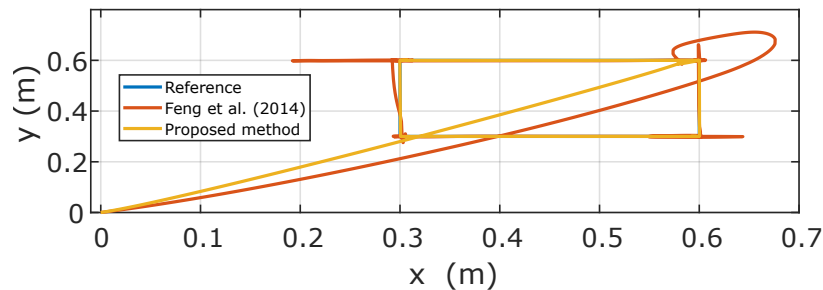


FIGURE 6 Simulation results showing the quadrotor trajectory performance in the 2D environment of each controller: control in Feng et al. (2014) (—) and proposed method (—) (Nominal model).

controllers proposed Feng et al. (2014)¹², Shi et al. (2019)⁴⁸, and Labbadi et al. (2020)⁴⁹. According to the quantitative analysis in Table 2, the suggested control results in decreased ISE error values for the quadrotor's position and orientation. The ISE values for the tracking errors are reduced when compared to the outcomes of the other procedures. These results all point to the suggested control method's ability to improve tracking performance in terms of high tracking precision, rapid reaction, fluid control commands, and high resilience. This study's control strategy has higher tracking control performance, which has been demonstrated. In terms of tracking precision, convergence speed, and resilience against disturbances, it performs better than other approaches. On the other hand, the integral absolute derivative control signal (IADU) index has been calculated for all control signals in the scenario 2. The smoothness of control signals can be easily determined using this performance metric. As shown in Table 3, the proposed method produces smoother input control signals than the alternative strategy, indicating the effectiveness of the proposed controller. The simulation's results are displayed in Table 3. It can be seen that the proposed control approach for all control signals enhances smoothness. Comparing the proposed control to the^{12, 48, and 49} techniques in

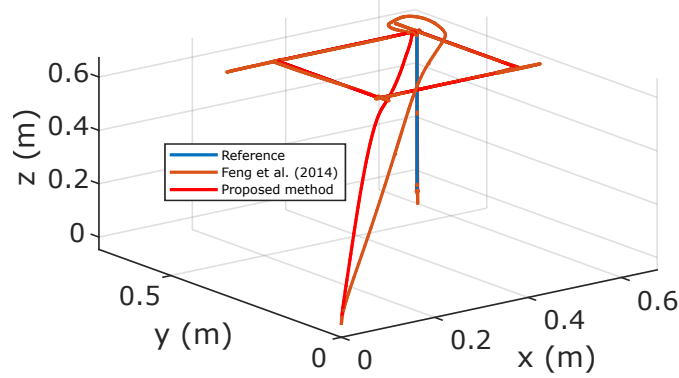


FIGURE 7 Simulation results showing the quadrotor trajectory performance in the 3D environment of each controller: control in Feng et al. (2014) (—) and proposed method (—) (Nominal model).

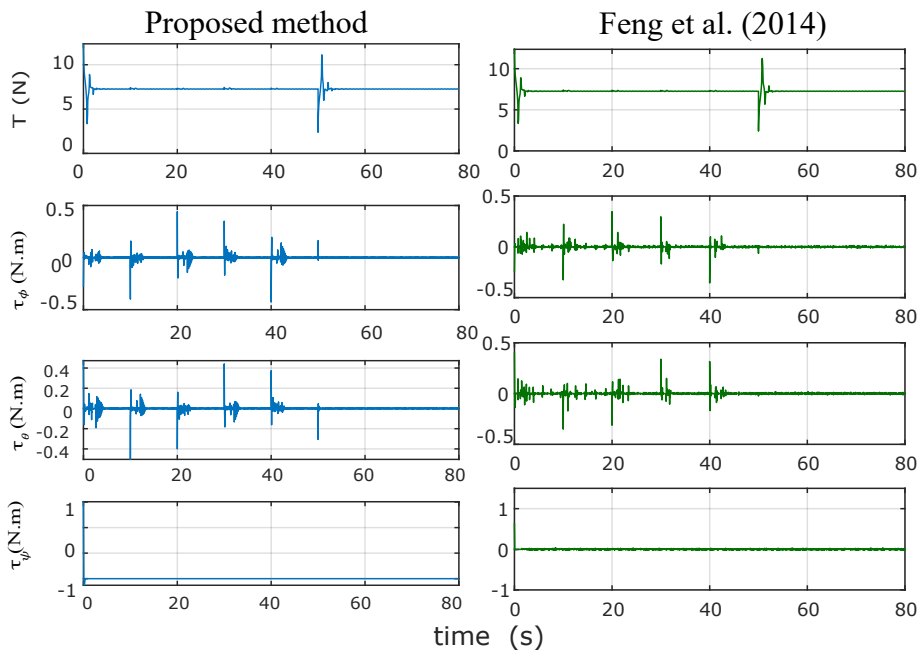


FIGURE 8 Simulation results showing the quadrotor control inputs control for each controller: control in Feng et al. (2014) (—) and proposed method (—) (Nominal model).

Table 3 it can be shown that the suggested control can ensure the least amount of transmission data controller-to-motor ends, considerably cutting consumption energy and lowering unnecessary expenditures.

6 | CONCLUSIONS

This paper proposed a FO command filtered-based recursive finite-time control using a nonsingular terminal sliding mode technique for high-order uncertain nonlinear systems under disturbances with unknown bounds. The proposed control is developed to get beyond the limitations of existing finite-time tracking controllers like the TSM control. Furthermore, in the proposed approach, the reaching phase is removed, the explosion of complexity in the control problem is avoided, and a chattering alleviation property is achieved. Then, this fractional-order strategy has been applied to control a quadrotor UAV system in different scenarios affected by increasing disturbance amplitudes and frequencies. This technique has been proved to be an appropriate

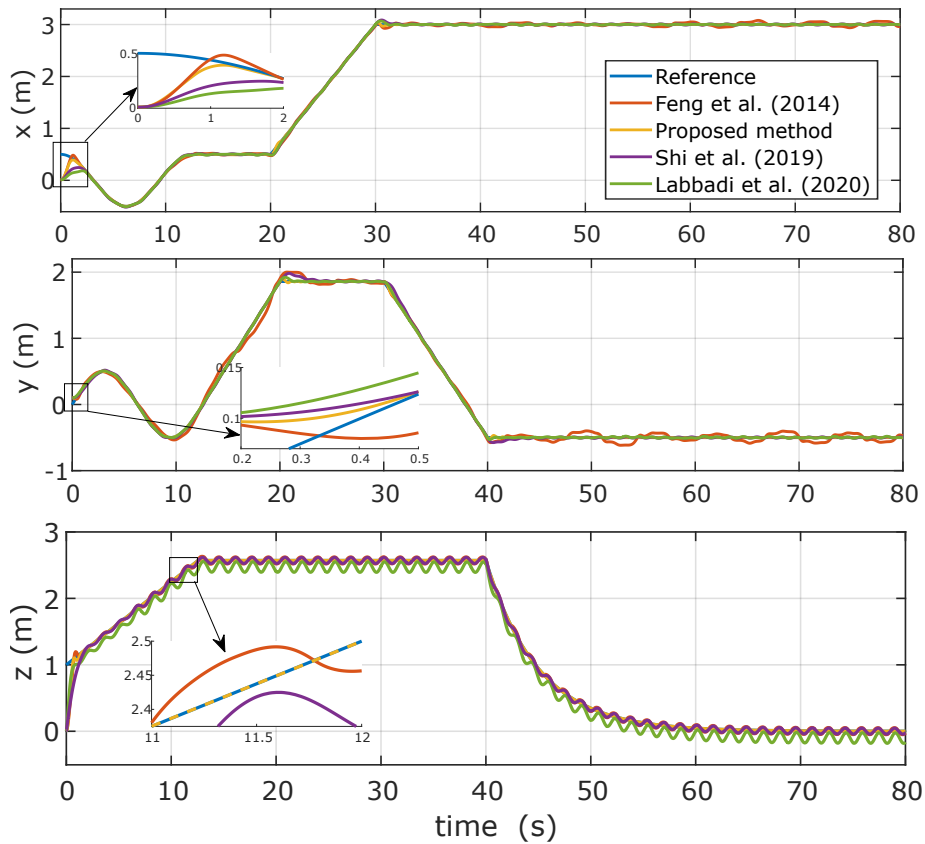


FIGURE 9 Simulation results showing the position performance of each controller: reference (—), control in Feng et al. (2014) (—), proposed method (—), control in Shi et al. (2019) (—), control in Labbadi et al. (2020) (—) (Increasing disturbance amplitudes).

TABLE 2 Indices de performance ISE of the scenario 2 (Increasing disturbance amplitudes)

Control signals	Proposed method	Control in ¹²	Control in ⁴⁸	Control in ⁴⁹
$x(t)$	0.1824	0.7673	0.1981	0.2123
$y(t)$	0.002	0.2617	0.0449	0.00811
$z(t)$	0.2718	0.4283	1.231	0.4345
$\psi(t)$	0.1111	0.2822	0.2822	0.2658
$\theta(t)$	0.0348	0.0373	0.0372	0.035
$\phi(t)$	0.0234	0.0344	0.0344	0.021

solution for controlling such systems and ensuring the needed tracking. Furthermore, simulation results have demonstrated the effectiveness of the proposal even in comparison with an existing approach in the literature.

As future work, we consider the situation where observers, controllers, and consensus algorithms all meet finite-time performance goals. Future research will focus on the proposed controller's adaptive mechanism. Future consideration will also be given to the extension to the examination of high-order systems' fixed-time stability.

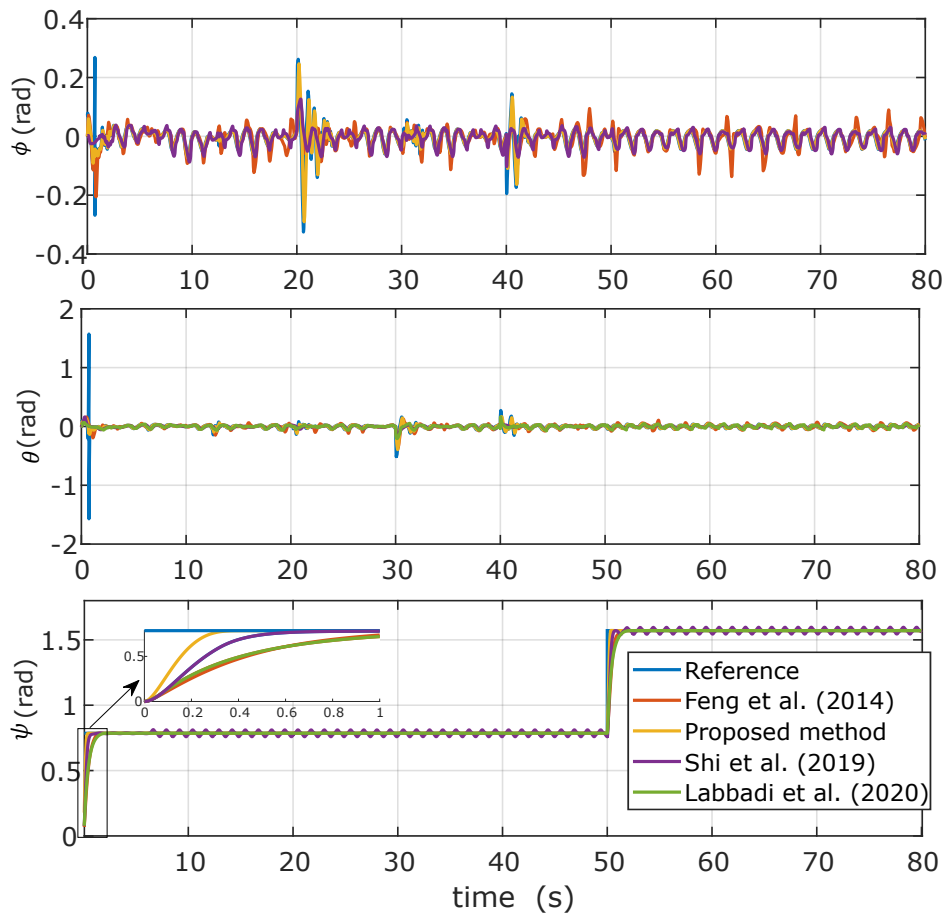


FIGURE 10 Simulation results showing the attitude performance of each controller: reference (—), control in Feng et al. (2014) (—), proposed method (—), control in Shi et al. (2019) (—), control in Labbadi et al. (2020) (—) (Increasing disturbance amplitudes).

TABLE 3 IADU index performance analysis of the scenario 2 (Increasing disturbance amplitudes)

Control signals	Proposed method	Control in ¹²	Control in ⁴⁸	Control in ⁴⁹
Total torques	0.0954	0.1033	0.1001	0.0959
Total thrust	6.3070	7.476	9.744	6.498

7 | BIBLIOGRAPHY

References

1. V. Utkin, (1977) Variable structure systems with sliding modes, IEEE Transactions on Automatic control, vol. 22, no. 2, pp. 212-222.
2. Y. Shtessel, C. Edwards, L. Fridman, and A. Levant (2014) Sliding mode control and observation, ser. Control Engineering. Birkh'auser.
3. V. Utkin and J. Shi (1996) Integral sliding mode in systems operating under uncertainty conditions," in 35th IEEE conference on decision and control, vol. 4. IEEE, pp. 4591-4596.

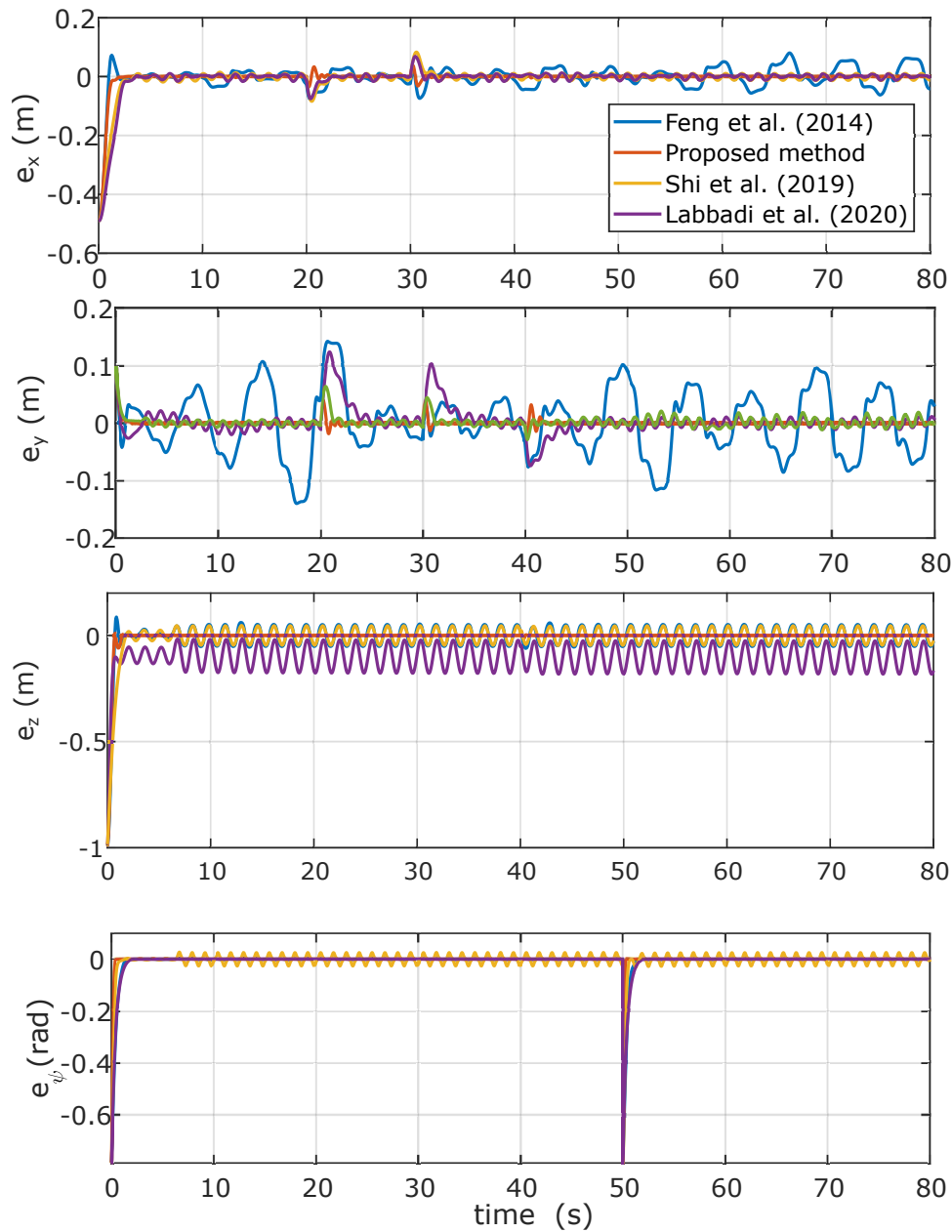


FIGURE 11 Simulation results showing the tracking errors performance of each controller: control in Feng et al. (2014) (—), proposed method (—), control in Shi et al. (2019) (—), control in Labbadi et al. (2020) (—) (Increasing disturbance amplitudes).

4. A. Ferrara, G. P. Incremona, and M. Cucuzzella, (2019) *Advanced and Optimization Based Sliding Mode Control: Theory and Applications*. Philadelphia, PA, USA: Society for Industrial and Applied Mathematics.
5. G. P. Incremona, M. Rubagotti and A. Ferrara, (2017) Sliding Mode Control of Constrained Nonlinear Systems. *IEEE Transactions on Automatic Control*, vol. 62, no. 6, pp. 2965-2972.
6. G. P. Incremona, L. Mirkin and P. Colaneri, (2022) Integral Sliding-Mode Control With Internal Model: A Separation. *IEEE Control Systems Letters*, vol. 6, pp. 446-451.
7. Bhat, S. P., Bernstein, D. S. (1997). Finite-time stability of homogeneous systems. In *Proc. American control conf* (pp. 1073-1078).

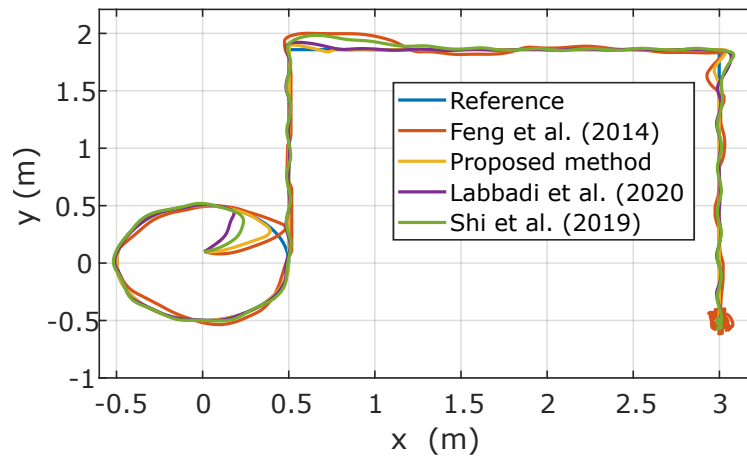


FIGURE 12 Simulation results showing the quadrotor trajectory performance in the 2D environment of each controller: control in Feng et al. (2014) (—), proposed method (—), control in Shi et al. (2019) (—), control in Labbadi et al. (2020) (—) (Increasing disturbance amplitudes).

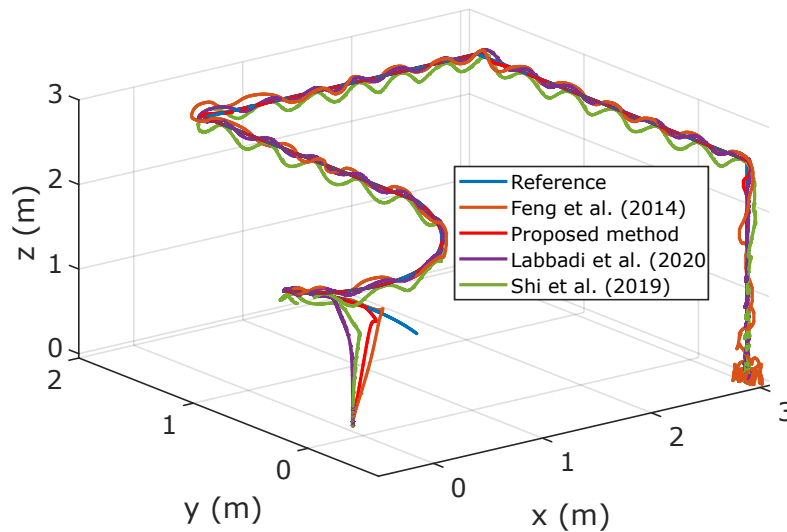


FIGURE 13 Simulation results showing the quadrotor trajectory performance in the 3D environment of each controller: control in Feng et al. (2014) (—), proposed method (—), control in Shi et al. (2019) (—), control in Labbadi et al. (2020) (—) (Increasing disturbance amplitudes).

8. Yu, X., Feng, Y., and Man, Z. (2020) Terminal Sliding Mode Control - An Overview. *IEEE Open J. Ind. Electron. Soc.*, 2, 36-52.
9. Feng, Y., Yu, X., and Man, Z. (2002) Non-singular terminal sliding mode control of rigid manipulators. *Automatica*, 38 (12), 2159-2167.
10. Feng, Y., Yu, X., and Han, F. (2013) *Automatica* On nonsingular terminal sliding-mode control of nonlinear systems. *Automatica*, 1-8.
11. S. Yu, X. Yu, B. Shirinzadeh, and Z. Man (2005) Continuous finite-time control for robotic manipulators with terminal sliding mode, *Automatica*, vol. 41, no. 11, pp. 1957-1964, 2005.
12. Feng, Y., Han, F., and Yu, X. (2014) Chattering free full-order sliding-mode control. *Automatica*, 50 (4), 1310-1314.

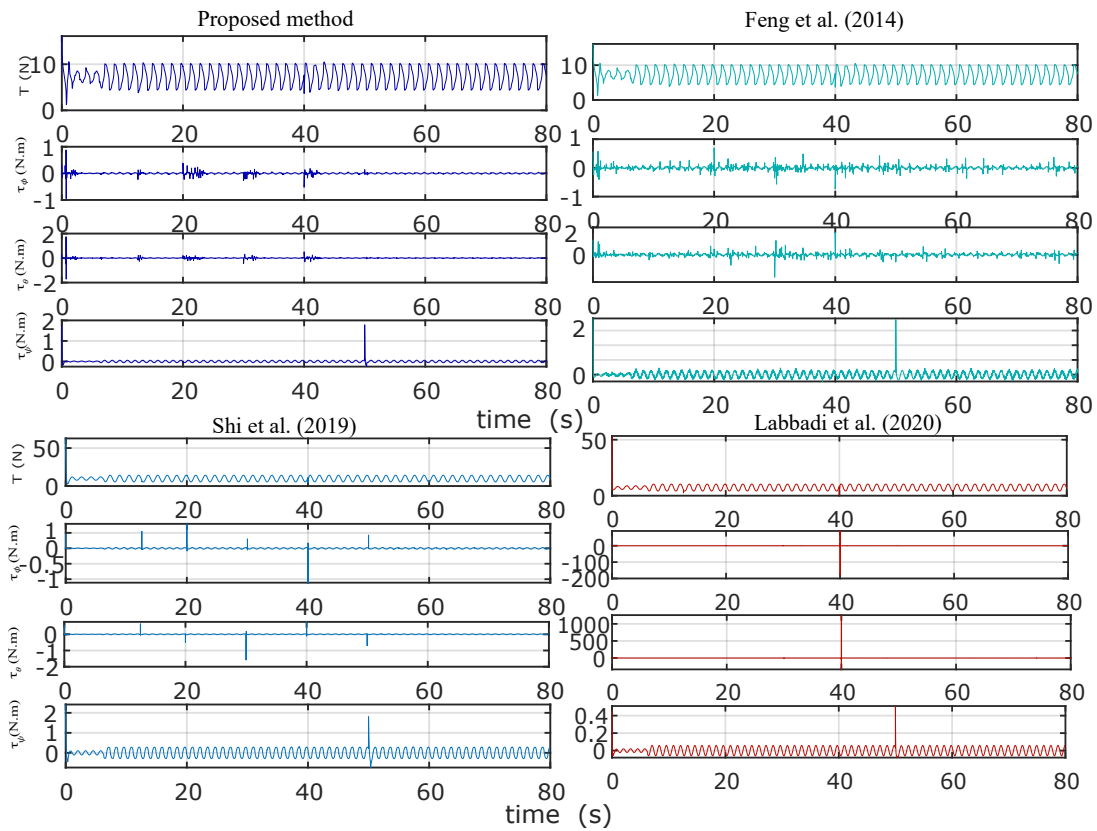


FIGURE 14 Simulation results showing the quadrotor control inputs: control in Feng et al. (2014) (—), proposed method (—), control in Shi et al. (2019) (—), control in Labbadi et al. (2020) (—) (Increasing disturbance amplitudes).

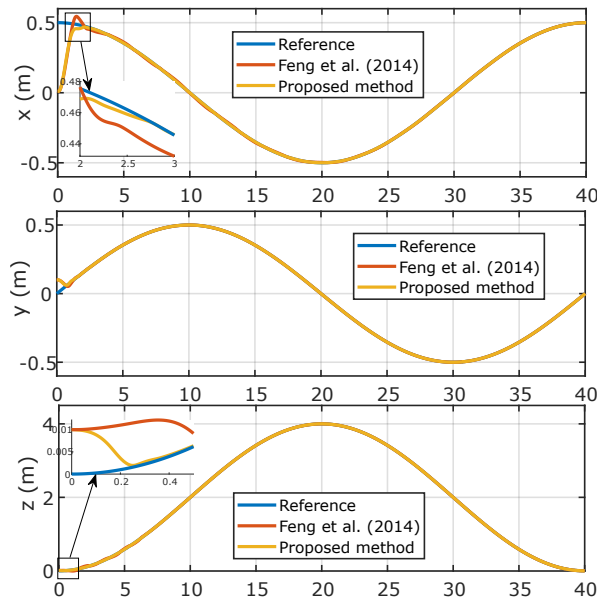


FIGURE 15 Simulation results showing the position performance of each controller: reference (—), control in Feng et al. (2014) (—), and proposed method (—) (Increasing disturbance frequencies).

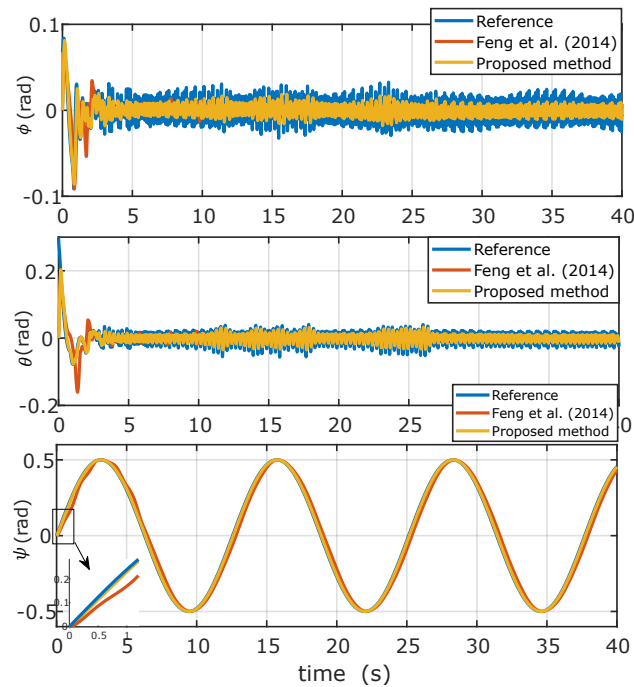


FIGURE 16 Simulation results showing the attitude performance of each controller; Reference (—), Feng et al. (2014) (—), and Proposed method (—) (Increasing disturbance frequencies).

14. Bartolini, G., Ferrara, A., and Usai, E. (1998). Chattering avoidance by second-order sliding mode control. *IEEE Transactions on Automatic Control*, 43(2), 241-246.
15. Levant, A. (1998). Robust exact differentiation via sliding mode technique. *Automatica*, 34(3), 379-384.
16. Shtessel, Y. B., Shkolnikov, I. A., and Brown, M. D. J. (2003). An asymptotic second-order smooth sliding mode control. *Asian Journal of Control*, 5(4), 498-504.
17. Shao, K., Zheng, J., Huang, K., Wang, H., Man, Z., and Fu, M. (2020) Finite-Time Control of a Linear Motor Positioner Using Adaptive Recursive Terminal Sliding Mode. *IEEE Trans. Ind. Electron.*, 67 (8), 6659-6668.
18. Song Z, Duan C, Wang J, Wu Q. Chattering-free full-order recursive sliding mode control for finite-time attitude synchronization of rigid spacecraft. *J Frankl Inst.* 2018;356(2):998-1020.
19. Utkin VI, Poznyak AS. Adaptive sliding mode control with application to super-twist algorithm: equivalent control method. *Automatica*. 2013;49(1):39-47.
20. Shtessel Y, Taleb M, Plestan F. A novel adaptive-gain supertwisting sliding mode controller: methodology and application. *Automatica*. 2012;48(5):759-769.
21. Plestan F, Taleb M, Bououlid B.. High order integral sliding mode control with gain adaptation. Paper presented at: Proceedings of the 2013 European Control Conference (ECC). Zurich, Switzerland; July 17, 2013:890-895; IEEE.
22. Zhu, Z. Liang, H. Liu, Y. Xue, H (2021) Command filtered event-triggered adaptive control for MIMO stochastic multiple time-delay systems. *I. J. of Rob. and Non. Cont.*, <https://doi.org/10.1002/rnc.5868>.
23. Han, S. (2020) Fractional-order command filtered backstepping sliding mode control with fractional-order nonlinear disturbance observer for nonlinear systems. *J. Franklin Inst.*, 357 (11), 6760-6776.
24. Song, S., Park, J.H., Zhang, B., Song, X., and Zhang, Z. (2021) Adaptive Command Filtered Neuro-Fuzzy Control Design for Fractional-Order Nonlinear Systems with Unknown Control Directions and Input Quantization. *IEEE Trans. Syst. Man, Cybern. Syst.*, 51 (11), 7238-7249.

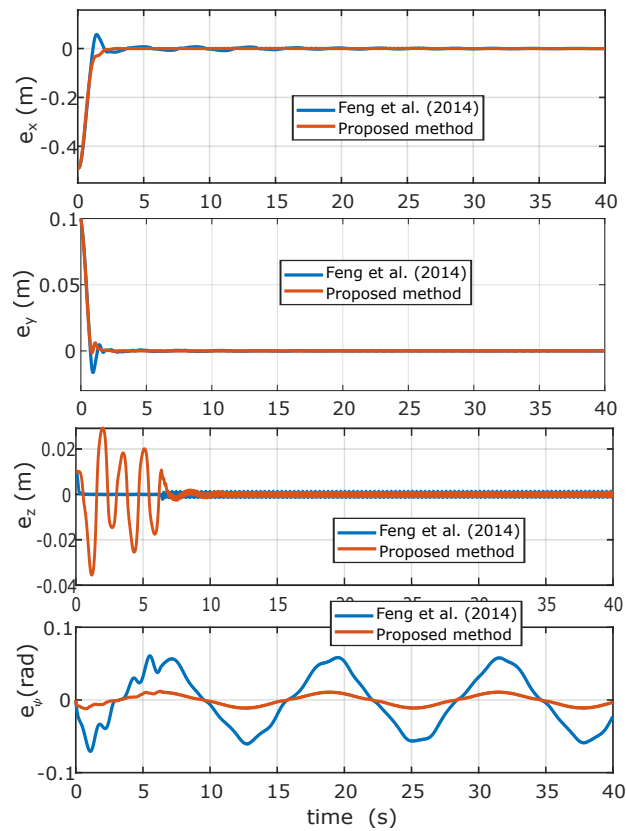


FIGURE 17 Simulation results showing the tracking errors performance of each controller; Feng et al. (2014) (—) and Proposed method (—) (Increasing disturbance frequencies).

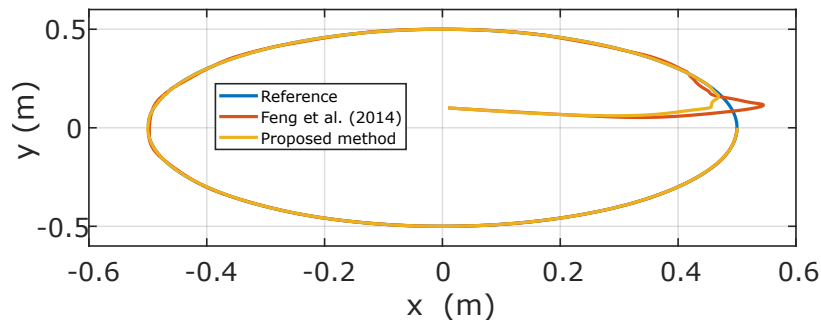


FIGURE 18 Simulation results showing the quadrotor trajectory performance in the 2D environment of each controller: control Feng et al. (2014) (—) and proposed method (—) (Increasing disturbance frequencies).

25. Ma, J., Park, J.H., and Xu, S. (2021) Command-Filter-Based Finite-Time Adaptive Control for Nonlinear Systems with Quantized Input. *IEEE Trans. Automat. Contr.*, 66 (5), 2339-2344.
26. Zhang, J., Xia, J., Sun, W., Wang, Z., and Shen, H. (2019) Command filter-based finite-time adaptive fuzzy control for nonlinear systems with uncertain disturbance. *J. Franklin Inst.*, 356 (18), 11270-11284.
27. Zhu, X., Ding, W., and Zhang, T. (2021) Command filter-based adaptive prescribed performance tracking control for uncertain pure-feedback nonlinear systems with full-state time-varying constraints. *Int. J. Robust Nonlinear Control*, 31 (11), 5312-5329.

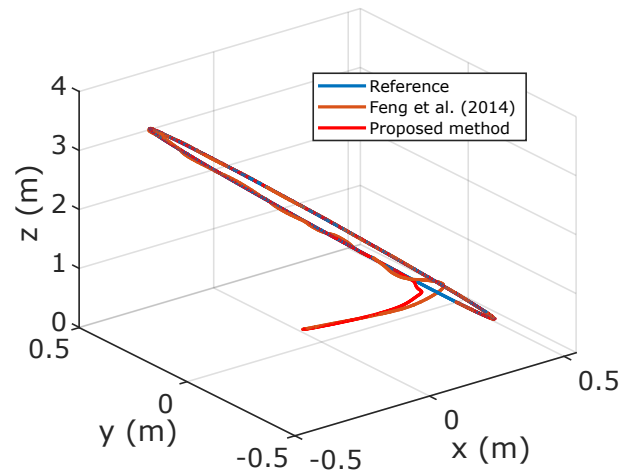


FIGURE 19 Simulation results showing the quadrotor trajectory performance in the 3D environment of each controller: Feng et al. (2014) (—), and proposed method (—) (Increasing disturbance frequencies).

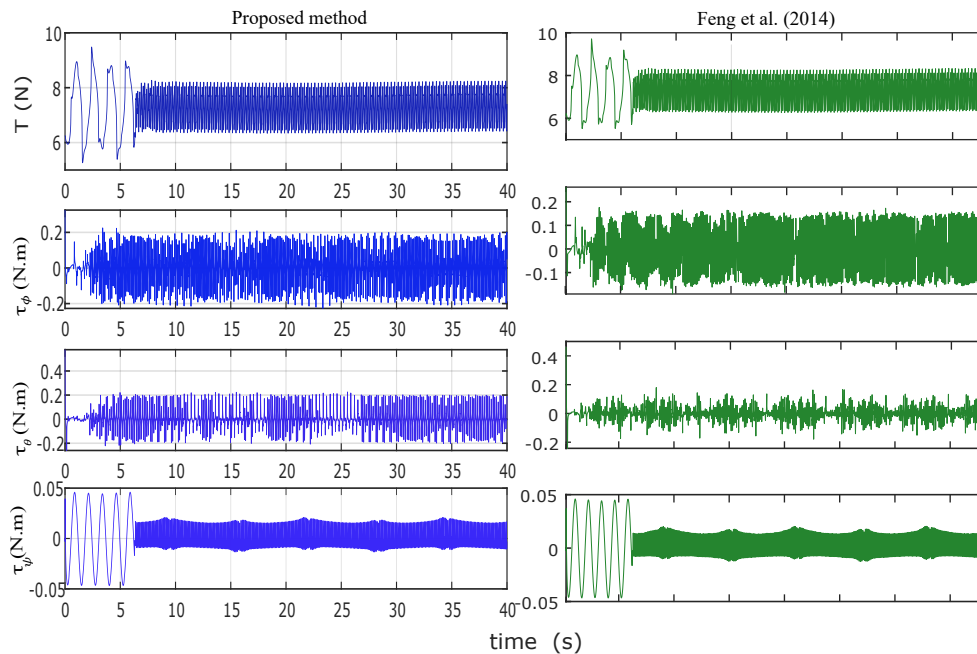


FIGURE 20 Simulation results showing the quadrotor control inputs of each controller: Feng et al. (2014) (—), and proposed method (—) (Increasing disturbance frequencies).

28. Wei, W., and Zhang, W. (2021) Command-Filter-Based Adaptive Fuzzy Finite-Time Output Feedback Control for State-Constrained Nonlinear Systems With Input Saturation. *IEEE Trans. Fuzzy Syst.*, 6706 (c), 1-1.
29. L. Chen, Z. Liu, Q. Dang, W. Zhao, G. Wang, Robust trajectory tracking control for a quadrotor using recursive sliding mode control and nonlinear extended state observer, *Aerosp. Sci. Technol.* 128 (2022) 107749. <https://doi.org/10.1016/j.ast.2022.107749>.
30. S. Wang, A. Polyakov, and G. Zheng, "Quadrotor stabilization under time and space constraints using implicit PID controller," *J. Franklin Inst.*, vol. 359, no. 4, pp. 1505-1530, 2022, doi: 10.1016/j.jfranklin.2022.01.002.
31. A. Romero, S. Sun, P. Foehn and D. Scaramuzza, "Model Predictive Contouring Control for Time-Optimal Quadrotor Flight," in *IEEE Transactions on Robotics*, 2022, doi: 10.1109/TRO.2022.3173711.

32. S. Sun, A. Romero, G. S. Member, P. Foehn, G. S. Member, and A. Motivation, "A Comparative Study of Nonlinear MPC and Differential-Flatness-Based Control for Quadrotor Agile Flight," in *IEEE Transactions on Robotics*, pp. 1-17, 2022.
33. D. He, "An α -variable model-free prescribed-time control for nonlinear system with uncertainties and disturbances," no. March 2021, pp. 5673-5693, 2022, doi: 10.1002/rnc.6105.
34. X. Gu, B. Xian, and Y. Wang, "Agile flight for a quadrotor via robust geometry control: Theory and experimental verification," no. January, pp. 4236-4250, 2022, doi: 10.1002/rnc.6022.
35. N. Vafamand, "Robust neural network-based backstepping landing control of quadrotor on moving platform with stochastic noise," no. December 2020, pp. 2007-2026, 2022, doi: 10.1002/rnc.5933.
36. K. Xia, M. Shin, W. Chung, M. Kim, S. Lee, and H. Son, "Control Engineering Practice Landing a quadrotor UAV on a moving platform with sway motion using robust control," *Control Eng. Pract.*, vol. 128, no. July, p. 105288, 2022, doi: 10.1016/j.conengprac.2022.105288.
37. L. Chen, Z. Liu, Q. Dang, W. Zhao, and G. Wang, "Robust trajectory tracking control for a quadrotor using recursive sliding mode control and nonlinear extended state observer," *Aerosp. Sci. Technol.*, vol. 128, p. 107749, 2022, doi: 10.1016/j.ast.2022.107749
38. Falcon, R., Rios, H., Dzul, A.: A sliding-mode-based active fault-tolerant control for robust trajectory tracking in quad-rotors under a rotor failure. *Int. J. Robust Nonlinear Control*. 2022;32 (15) 8451-8469 doi.org/10.1002/rnc.6288
39. Zhao, J.; Ding, X.; Jiang, B.; Jiang, G.; Xie, F. A novel sliding mode fault-tolerant control strategy for variable-mass quadrotor. *Int. J. Robust Nonlinear Control* 2022, 1, 1-28 doi.org/10.1002/rnc.6159
40. Reis J , Yu G , Cabecinhas D, Silvestre C High-performance quadrotor slung load transportation with damped oscillations . *Int. J. Robust Nonlinear Control* 2022, 1, 1-30 doi.org/10.1002/rnc.6306
41. Liu, H.; Li, B.; Xiao, B.; Ran, D.; Zhang, C. Reinforcement learning-based tracking control for a quadrotor unmanned aerial vehicle under external disturbances. *Int. J. Robust Nonlinear Control* 2022;1-18 doi.org/10.1002/rnc.6334
42. I. Podlubny, *Fractional Differential Equations*. New York: Academic, 1999.
43. S. Das, *Functional Fractional Calculus for System Identification and Controls*. Heidelberg: Springer-Verlag, 2008.
44. I. Podlubny, Geometric and physical interpretation of fractional integration and fractional differentiation, *Fractional Calculus & Applied Analysis*, vol. 5, pp. 367-386, 2002.
45. Shao K. Nested adaptive integral terminal sliding mode control for high-order uncertain nonlinear systems. *Int J Robust Nonlinear Control*. 2021;31:6668-6680. <https://doi.org/10.1002/rnc.5631>.
46. M. Labbadi and M. Cherkaoui, (2020) Robust adaptive nonsingular fast terminal sliding-mode tracking control for an uncertain quadrotor UAV subjected to disturbances, *ISA Trans.*, vol. 99, pp. 290-304, 2019.. 540-544.
47. F.P. Freire, N.A. Martins, F. Splendor, A Simple Optimization Method for Tuning the Gains of PID Controllers for the Autopilot of Cessna 182 Aircraft Using Model-in-the-Loop Platform, *J. Control. Autom. Electr. Syst.* 29 (2018) 441-450. <https://doi.org/10.1007/s40313-018-0391-x>.
48. X. Shi, Y. Cheng, C. Yin, S. Dadras, X. Huang, Design of Fractional-Order Backstepping Sliding Mode Control for Quadrotor UAV, *Asian J. Control*. 21 (2019) 156-171. <https://doi.org/10.1002/asjc.1946>.
49. M. Labbadi, M. Cherkaoui, Robust adaptive nonsingular fast terminal sliding-mode tracking control for an uncertain quadrotor UAV with disturbances, *ISA Trans.* (2019) 1-52. <https://doi.org/10.1016/j.isatra.2019.10.012>.